Ateneo de Manila University

Archīum Ateneo

Physics Faculty Publications | Physics Department

2017

Quantification of urban atmospheric boundary layer greenhouse gas dry mole fraction enhancements in the dormant season: Results from the Indianapolis Flux Experiment (INFLUX)

Natasha Miles

Scott Richardson

Thomas Lauvaux

Kenneth J. Davis

Nikolay V. Balashov

See next page for additional authors

Follow this and additional works at: https://archium.ateneo.edu/physics-faculty-pubs

 Part of the Atmospheric Sciences Commons

Authors

Natasha Miles, Scott Richardson, Thomas Lauvaux, Kenneth J. Davis, Nikolay V. Balashov, Aijun Deng, Jocelyn Turnbull, Colm Sweeney, Kevin R. Gurney, Risa Patarasuk, Igor Razlivanov, Maria Obiminda L. Cambaliza, and Paul B. Shepson

ELEMENTA
Science of the Anthropocene

Miles, NL, et al 2017 Quantification of urban atmospheric boundary layer greenhouse gas dry mole fraction enhancements in the dormant season: Results from the Indianapolis Flux Experiment (INFLUX). *Elem Sci Anth,* 5: 27, DOI: https://doi.org/10.1525/elementa.127

RESEARCH ARTICLE

Quantification of urban atmospheric boundary layer greenhouse gas dry mole fraction enhancements in the dormant season: Results from the Indianapolis Flux Experiment (INFLUX)

Natasha L. Miles[*], Scott J. Richardson[*], Thomas Lauvaux[*], Kenneth J. Davis[*], Nikolay V. Balashov[*], Aijun Deng[*], Jocelyn C. Turnbull[†,‡], Colm Sweeney[‡], Kevin R. Gurney[§], Risa Patarasuk[§], Igor Razlivanov[§], Maria Obiminda L. Cambaliza[‖,¶] and Paul B. Shepson[‖]

We assess the detectability of city emissions via a tower-based greenhouse gas (GHG) network, as part of the Indianapolis Flux (INFLUX) experiment. By examining afternoon-averaged results from a network of carbon dioxide (CO_2), methane (CH_4), and carbon monoxide (CO) mole fraction measurements in Indianapolis, Indiana for 2011–2013, we quantify spatial and temporal patterns in urban atmospheric GHG dry mole fractions. The platform for these measurements is twelve communications towers spread across the metropolitan region, ranging in height from 39 to 136 m above ground level, and instrumented with cavity ring-down spectrometers. Nine of the sites were deployed as of January 2013 and data from these sites are the focus of this paper. A background site, chosen such that it is on the predominantly upwind side of the city, is utilized to quantify enhancements caused by urban emissions. Afternoon averaged mole fractions are studied because this is the time of day during which the height of the boundary layer is most steady in time and the area that influences the tower measurements is likely to be largest. Additionally, atmospheric transport models have better performance in simulating the daytime convective boundary layer compared to the nighttime boundary layer. Averaged from January through April of 2013, the mean urban dormant-season enhancements range from 0.3 ppm CO_2 at the site 24 km typically downwind of the edge of the city (Site 09) to 1.4 ppm at the site at the downwind edge of the city (Site 02) to 2.9 ppm at the downtown site (Site 03). When the wind is aligned such that the sites are downwind of the urban area, the enhancements are increased, to 1.6 ppm at Site 09, and 3.3 ppm at Site 02. Differences in sampling height affect the reported urban enhancement by up to 50%, but the overall spatial pattern remains similar. The time interval over which the afternoon data are averaged alters the calculated urban enhancement by an average of 0.4 ppm. The CO_2 observations are compared to CO_2 mole fractions simulated using a mesoscale atmospheric model and an emissions inventory for Indianapolis. The observed and modeled CO_2 enhancements are highly correlated (r^2 = 0.94), but the modeled enhancements prior to inversion average 53% of those measured at the towers. Following the inversion, the enhancements follow the observations closely, as expected. The CH_4 urban enhancement ranges from 5 ppb at the site 10 km predominantly downwind of the city (Site 13) to 21 ppb at the site near the landfill (Site 10), and for CO ranges from 6 ppb at the site 24 km downwind of the edge of the city (Site 09) to 29 ppb at the downtown site (Site 03). Overall, these observations show that a dense network of urban GHG measurements yield a detectable urban signal, well-suited as input to an urban inversion system given appropriate attention to sampling time, sampling altitude and quantification of background conditions.

Keywords: urban; greenhouse gas; carbon dioxide; methane; tower; in-situ

[*] Department of Meteorology, The Pennsylvania State University, University Park, Pennsylvania, US

[†] National Isotope Centre, GNS Science, Lower Hutt, NZ

[‡] National Oceanic and Atmospheric Administration/University of Colorado, Boulder, Colorado, US

[§] Arizona State University, Tempe, Arizona, US

[‖] Purdue University, West Lafayette, Indiana, US

[¶] Ateneo de Manila University, Katipunan Ave, Quezon City, Metro Manila, Philippines 1108, PH

Corresponding author: Natasha L. Miles (nmiles@psu.edu)

1 Introduction

Atmospheric greenhouse gas (GHG) mole fractions continue to rise rapidly (currently at about 2.5 ppm/year), primarily in response to anthropogenic emissions from fossil fuel consumption (IPCC 2014). Of these anthropogenic emissions, about 70% originate from urban areas (IEA 2008). Climate change mitigation will require reductions of GHG emissions, thus the ability to quantify urban GHG emissions is essential for assessing the effectiveness of mitigation efforts.

Quantification of anthropogenic GHG emissions is traditionally accomplished via "bottom-up" accounting or inventory methods (e.g. Marland et al., 1985; Andres et al., 1999). Interest in evaluating emissions at regional scales has motivated the development of spatially-distributed (CDIAC, Andres et al., 1999) and more temporally-resolved CO_2 emissions products (Vulcan, Gurney et al., 2009; Hestia, Gurney et al., 2012). A broadly utilized air quality emissions product, the Emission Database for Global Atmospheric Research, (EDGAR, European Commission JRC/PBL, 2013) provides a global assessment of spatially-resolved CH_4 (as well as CO_2 and other GHG) emissions. Most recently, a number of global products have used night lights and other remote sensing techniques to develop spatially-distributed emissions estimates (Oda and Maksyutov 2011; Rayner et al., 2010), sometimes including an uncertainty assessment (Asefi-Najafabady et al., 2014). All of these products use the same large-scale data utilized in national inventory products, but take a variety of approaches to distribute these emissions in space and time.

Inventory approaches are rich in information about sectoral emissions and spatial distribution, but challenging to assemble and maintain over time, and vulnerable to systematic errors (Marland and Boden, 1993; Turnbull et al., 2015). For the purposes of evaluating the effectiveness of voluntary or enforced mitigation efforts to reduce GHG emissions, independent assessment of anthropogenic GHG emissions is critical (Pacala et al., 2010; Nisbet and Weiss, 2010; Ciais et al, 2010; Durant et al., 2011). It is not yet clear what degree (resolution, precision, accuracy) of independent verification will be required. Regulations, however, are likely to be applied by sector (e.g., manufacturing sources, power generation sources, mobile sources), and thus highly resolved, accurate and precise emissions estimates from urban areas would be ideal for evaluation of emissions inventories and mitigation progress.

Atmospheric methods can potentially provide an independent assessment of emissions for cities. Depending on the objectives (trend detection, interannual variability, whole-city emissions, spatially resolved fluxes), different approaches are more or less suitable. Total emissions from an urban area have been obtained via an aircraft-based mass balance approach, comparing background and downwind mole fractions (Mays et al., 2009; Cambaliza et al., 2014; Cambaliza et al., 2015). The temporal coverage is, however, limited with aircraft, and downwind measurements alone provide little information about spatial patterns of fluxes within an urban region. Sensitivity analyses showed that the aircraft-based estimates of CO_2 and CH_4 emissions are most dependent upon determination of the appropriate background mole fraction (Cambaliza et al., 2015).

A number of experiments have been initiated in an attempt to demonstrate quantification of urban GHG emissions using tower- or building-based atmospheric approaches. McKain et al. (2012) compared simulated CO_2 mole fractions to five observational sites located in and around Salt Lake City, Utah. They argued that the similarity between observed and simulated CO_2 suggested that urban inversions are possible. The temporal duration of the study was limited to four 3–5 week time periods in 2006, and the primary focus was on the amplitude of the diurnal cycle in the region. McKain et al. (2014) solved for methane (CH_4) emissions from the city of Boston using a network of five tower and building-based observations. This study optimized whole-city emissions and did not evaluate spatial structure of emissions within the city. These studies have shown promise in quantifying whole city emissions but have not yet demonstrated the ability to resolve emissions in space, and have had limited ability to explore the sensitivity of their findings to the layout of their observational networks. Extensive networks of greenhouse gas measurements have also been implemented in Paris, France (Bréon et al., 2015), and Los Angeles, California (Verhulst et al., 2017).

Lauvaux et al. (2013) implemented a simplified version of an inversion approach to determine, in real-time, changes in the CO_2 emissions for the city of Davos, Switzerland, using an atmospheric transport model and two CO_2 measurement sites. This simple approach provided information about temporal changes in GHG emissions, but did not quantify total emissions. Further, a single measurement site is sensitive to changes in the spatial distribution within an urban region that is not representative of the whole-city emissions.

Finally, spatially- and temporally-resolved GHG emissions can be quantified with frequent, spatially-distributed measurements of GHG mole fractions merged with an atmospheric transport model and a method of solving for those fluxes most consistent with the measured and modeled GHG mole fractions. This atmospheric inversion approach has been used successfully to determine spatially- and temporally-resolved emissions consistent with agricultural inventory results in the U.S. Upper Midwest (Schuh et al., 2013; Lauvaux et al., 2012), and has been applied to Indianapolis (Lauvaux et al., 2016).

The first step towards implementing the atmospheric inversion approach at high resolution is assessing the detectability of the city emission flux via the tower-based GHG network, and documenting the spatial and temporal patterns. Here we present results from a dense network of highly-calibrated GHG sensors deployed in an urban area, as part of the Indianapolis Flux (INFLUX) experiment. This study provides a description of multi-species variability of atmospheric GHGs along with the high spatial and temporal resolution we expect to be needed to fully characterize and quantify urban emissions across space, time, and economic sectors in a large metropolitan area. We assess the detectability of city emissions via the tower-based GHG

network, and quantify the spatial and temporal patterns in atmospheric GHG mole fractions associated with the urban emissions. We further compare the observed CO_2 mole fraction enhancements across the city to those predicted by a numerical modeling system that includes an inventory-based emissions estimate and an atmospheric transport model. This comparison tests the degree to which the observed CO_2 enhancements are similar to those expected from prior knowledge of emissions and atmospheric transport. Finally, we examine the sensitivity of the CO_2 results to variability in sampling height and time.

2 Methods

2.1 Study site

The study site is Indianapolis, Indiana, a medium-sized city in the Midwestern U.S. The population of Marion county, encompassing the majority of the urban area, for 2013 is 928,000 (U.S. Census Bureau; http://quickfacts.census.gov). According to the Vulcan national carbon dioxide emissions inventory (Gurney et al., 2009), the fossil fuel CO_2 emissions of Marion county are 4.3 MtC for 2013 (2014 release). Indianapolis is relatively isolated from other metropolitan areas, and agriculture is the predominant land cover type surrounding the city, except to the south, which is considerably forested (**Figure 1**). The terrain is relatively flat. The Hestia bottom-up fossil fuel CO_2 high-resolution inventory product (Gurney et al., 2012) is available for Indianapolis (Marion County) and the eight surrounding counties, providing a spatially and temporally resolved prior for top-down methods in order to evaluate and improve uncertainties in both inventories and inversions, a primary goal of INFLUX.

A map of INFLUX ground-based measurement sites and the city of Indianapolis is shown in **Figure 2**. The location, deployment date and measurements of the INFLUX sites are listed in **Table 1**, as are the known nearby sources of CO_2, CH_4, and CO. The predominant wind direction during the dormant season is from the southwest, although it varies considerably (**Figure 3**). The Harding Street Power Plant, contributing 28% of the CO_2 emissions of the city in 2002 (Gurney et al., 2012), is located in the southwest sector of the city. Between 2011 – 2013, the average monthly net electricity generation of the Harding Street Power Plant is 325,100 MWH (U.S. Energy Information Administration, 2016). During the study period, its primary fuel source is coal, but as of March 2016, its conversion to a natural gas facility was complete. There are several smaller power plants in the area as well: The Noblesville Station Power Plant (45,800 MWH average monthly generation; U.S. Energy Information Administration, 2016), 6 km to the north of Site 08, operates on steam generated from the hot exhaust of three combustion turbines fueled by natural gas. The C.C. Perry Power Plant (800 MWH mean monthly generation) is 2 km to the south of Site 03, and is primarily coal-fired during the study period but switched to natural gas in May 2014. The Eagle Valley Power Plant (109,400 MWH mean monthly generation for the period January – August 2011; 33,200 MWH mean monthly generation for September 2011 – December 2013; U.S. Energy Information Administration, 2016) is located 10 km to the south of Site 01 and is coal-fired with plans to be converted to a natural gas facility. Landfills and wastewater treatment plants are also indicated on the map (**Figure 2**). The South Side Landfill is located 6 km to the west of Site 10, and contributes 37% of the CH_4 emissions of the city (Cambaliza et al., 2015). The in-situ measurement sites were chosen such that Site 01 is the background site and Site 02 on the downwind edge of the city when the wind is from the predominant southwesterly direction. Site 09 is further downwind of the urban area, but depending on the wind direction, is another potential background site.

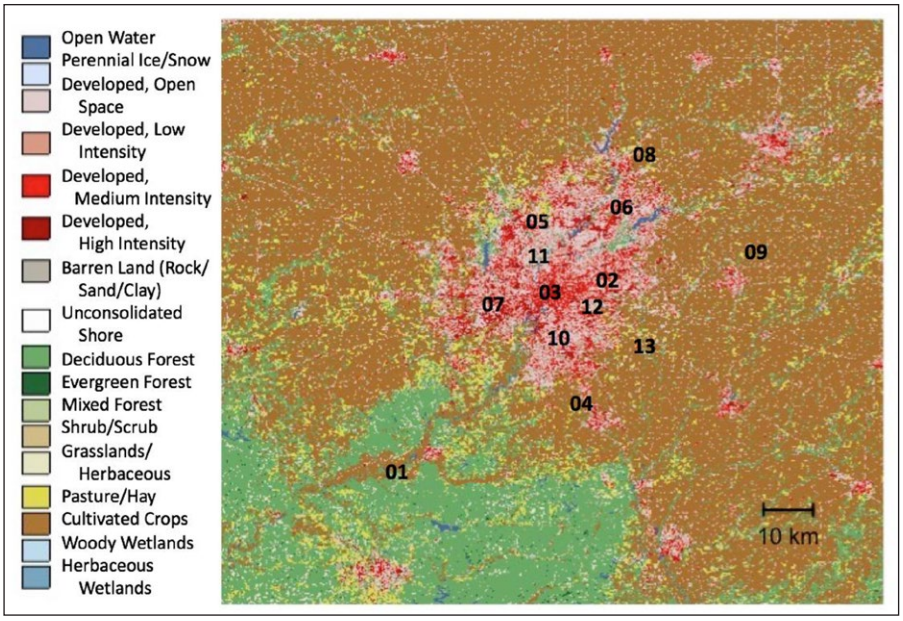

Figure 1: Land cover types for Indianapolis and the surrounding area. (National Land Cover Database 2011; Jin et al., 2013). The numbers 01–13 indicate tower site locations as listed in Table 1. DOI: https://doi.org/10.1525/elementa.127.f1

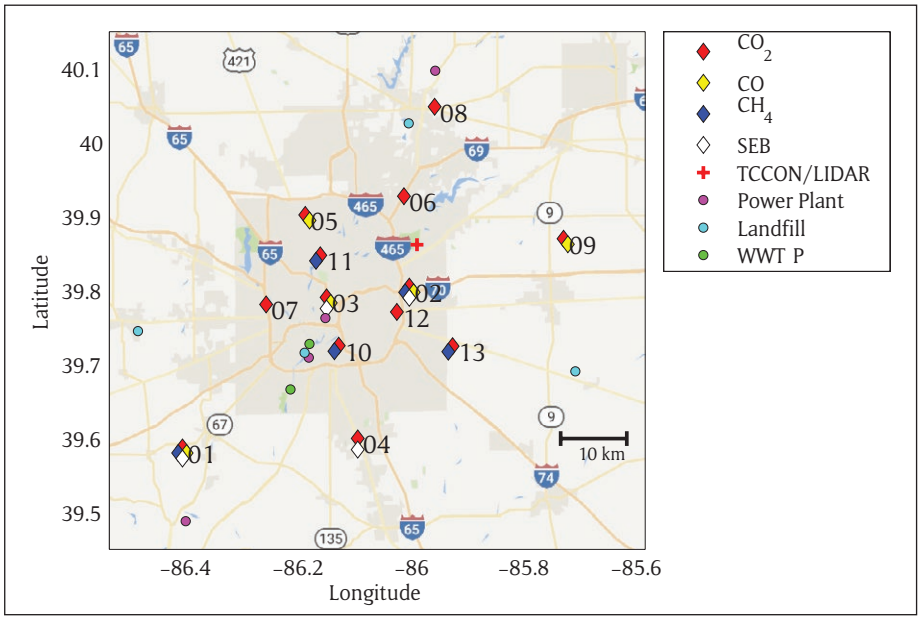

Figure 2: Map of the Indianapolis, IN, region, with INFLUX sites (as of January 2013) shown. The numbers 01–13 indicate tower site locations as listed in Table 1. The color of the marker represents the measurements at each site: red for CO_2, yellow for CO + NOAA flasks, blue for CH_4, and white for surface energy balance (SEB) fluxes. A NASA (Total Carbon Observing Network Fourier Transform Infrared) TCCON FTIR spectrometer was deployed from August – December 2012 at the site denoted by a red cross; a scanning Doppler lidar was deployed at the same site beginning in April 2013. Power plants, landfills, and wastewater treatment plants (WWTP) are indicated as well. The largest power plant is Harding Street and the largest landfill is South Side; both of these are located to the west of Site 10. Background road map: Google maps, www.google.com/maps. DOI: https://doi.org/10.1525/elementa.127.f2

Site 10 is closest to the primary power plant and landfill for the city. Site 03 is located near the downtown area, about 2 km from the center, and adjacent to a junction of two major interstate highways. Site 04 and Site 08, in particular, are 20 – 30 km from downtown, but in suburban/commercial areas of Indianapolis, and have light to medium urban development. The remaining sites are distributed around the city. Site 12 was deployed for only six months; the instrument was then relocated to a different site. The distance between each of the site-pairs (**Figure 2**) varies from 4 km (Site 02 and Site 12) to 66 km (Site 01 and Site 09).

2.2 Instrumentation

The INFLUX in-situ observation network includes twelve sites measuring CO_2 dry mole fractions. A subset of five sites additionally measure CO dry mole fraction, and a different subset of five sites additionally measure CH_4 dry mole fraction. In November 2014, four sites were upgraded from CO_2 only to CO_2 and CH_4 measurements. Measurements at two sites began in September 2010, seven sites were operational by August 2012, and nine of the sites were deployed as of January 2013 and data from these sites are the focus of this paper. The full network of twelve sites was deployed by July 2013. CO_2, CH_4, and CO dry mole fractions are measured with wavelength-scanned cavity ring down spectroscopic (CRDS) instruments (Picarro, Inc., models G2301, G2302, G2401, and G1301).

The instruments are deployed at the base of existing communications towers, with sampling tubes installed as high as possible on each tower (**Table 1**). Five of the tower measurement heights are greater than 100 m AGL, four are about 40 m AGL, and the remainder of the tower measurement heights are between 54 and 87 m AGL. Except for Site 03, the mean building height within the 1-km^2 area surrounding each of the towers is less than 6 m AGL and the measurements are thus expected to be above the roughness sublayer (typically 2 – 5 times the building height) most of the time. Site 03 is the closest of the INFLUX towers to the urban center, but it is about 2 km north of downtown. The tallest building in downtown Indianapolis is the Salesforce tower which is 247 m AGL and the remainder of the 20 tallest buildings are 79 – 162 m AGL (https://www.emporis.com/statistics/tallest-buildings/city/101039/indianapolis-in-usa). The buildings over 1 – 2 stories tall within a 300 m radius of the Site 03 tower are three Indiana University buildings about 70 – 150 m to the southwest which are 25 – 29 m tall and the Stutz Business Center 250 m to the southeast which is 21 m tall. The measurements may thus be within the roughness sublayer when the wind is from the southeast or southwest. The predominant landcover in the 1 km^2 area surrounding each tower is listed in **Table 1**. Sites 01, 05, 08, 09, and 11 have wooded landcover in the surrounding 1 km^2 area. Of these towers, Site 01, 05, 09, and 11 are all greater than 120 m AGL. Site 08, with about 10% wooded landcover, is 41 m AGL, and thus may at times be within the roughness sublayer. Sites 01, 02, and 03 also include measurements at 10 m AGL and one or two intermediate levels. Tubing for levels not being sampled is continuously purged in order to eliminate long residence times for the air in the tubing. The samples at all sites

Table 1: Details of INFLUX in-situ tower sites. Measurements are listed for the period of focus for this paper (2013). The CO_2 only sites were upgraded to measure both CO_2 and CH_4 in November 2014. DOI: https://doi.org/10.1525/elementa.127.t1

Site	Measurements	Installation date	Lat (deg N)	Long (deg W)	Sample height(s) (m AGL)	Known nearby sources	Predominant land-cover (in 1 km² surrounding tower)
*Site 01 – Background	CO_2/CO/CH_4/Flasks	9/2010	39.5805	86.4207	10/40/121	Power plant 10 km to the S	Wooded, sparse residential, agriculture
*Site 02 – Downwind edge	CO_2/CO/CH_4/Flasks	9/2010	39.7978	86.0183	10/40/136	I–70 200 m to the N	Residential, light commercial
*Site 03 – Downtown	CO_2/CO/Flasks	6/2012	39.7833	86.1651	10/20/40/54	I65–S 10 m to the SW; I65–N 40 m to the NE; power plant 2 km to the S	Commercial, residential, 2 km N of city center
*Site 04 – South Side	CO_2	8/2012	39.5927	86.0991	60		Light commercial, residential, agriculture
*Site 05 – NorthWest corner	CO_2/CO/Flasks	3/2012	39.8949	86.2028	125		Wooded, residential, apartment buildings
Site 06 – NorthEast corner	CO_2	7/2013	39.9201	86.0280	39	I–69 500 m to the NW; I–465 4 km to the SW	Light commercial, residential
*Site 07 – West Side	CO_2	3/2012	39.7739	86.2724	58	I465 200 m to the W	Residential, apartment buildings, light commercial
Site 08 – NorthEast	CO_2/CO/CH_4	5/2013	40.0411	85.9734	41	Power plant 6 km to the N	Agricultural, wooded
*Site 09 – Downwind/Background	CO_2/CO/Flasks	3/2012	39.8627N	85.7448W	10/40/70/130		Agricultural, golf course, wooded
*Site 10 – Downtown – South	CO_2/CH_4	3/2012	39.7181N	86.1436W	40	Landfill and power plant 6 km to the W	Warehouses, residential, light commercial
*Site 11 – Downtown – North	CO_2/CH_4	4/2013	39.8403N	86.1763W	130		Residential, university buildings, wooded, athletic fields, pond
*Site 12 – decommissioned 4/2013	CO_2	8/2012	39.7637N	86.0403W	40	4-lane roads 400m to the W and 1 km to the N; I465 800 m to the E	Residential, light commercial
*Site 13 – South East	CO_2/CH_4	4/2013	39.7173N	85.9417W	87		Agriculture, residential

*Results from these towers are presented in this manuscript.

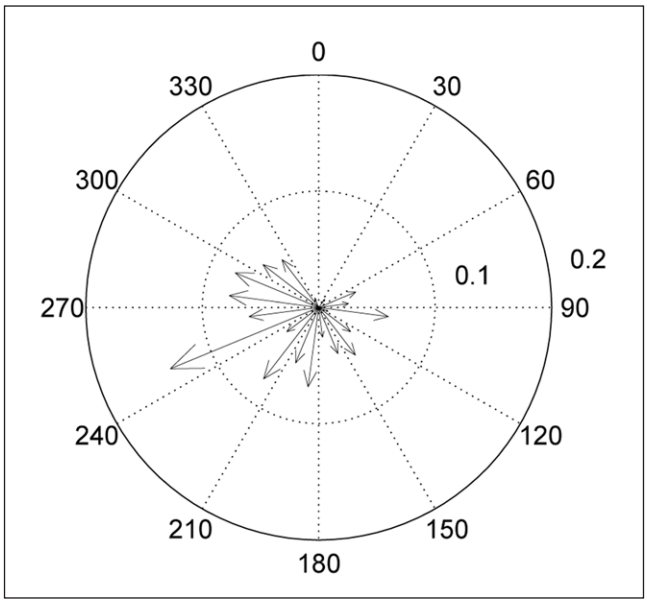

Figure 3: Probability distribution function of afternoon-averaged near-surface wind direction for 1 January – 30 April 2013. Wind direction is measured at the Indianapolis International airport (http://cdo.ncdc.noaa.gov/qclcd/QCLCD). Arrows point in the direction of origin of the afternoon-averaged mean winds. The radial length of the arrow denotes the fractional probability of wind from that direction. Wind directions are not reported for periods in which the wind speed is less than 1.6 ms^{-1}. DOI: https://doi.org/10.1525/elementa.127.f3

measuring CO have been dried since installation, to water vapor levels less than 0.6% at Site 02 and less than 0.2% at the other sites. As of late May 2013, the incoming sample air at all INFLUX sites is dried. Details of the air sampling systems at the INFLUX tower sites are described in Richardson et al. (2016).

Flow rates are approximately 240 cc min^{-1} for the G2301, G2302, and G2401 instruments and approximately 140 cc min^{-1} for the G1301 instruments. The measurement times are adjusted to reflect the residence time in the tubing (3–9 min for the top levels). For sites measuring at multiple heights, the 10-m and intermediate levels are each measured for 10 min of each hour, and the top level is sampled for the remainder of the hour. Four minutes of data are ignored after each transition between measurement levels and to/from field calibration gases, in order to flush the sample line.

The inter-laboratory compatibility goals set by the Global Atmosphere Watch program of the World Meteorological Organization are ±0.1 ppm CO_2 in the Northern Hemisphere and ±0.05 ppm CO_2 in the Southern Hemisphere, ±2 ppb CH_4, and ±2 ppb CO in background conditions and ±5 ppb CO in urban environments (GAW Report No. 229; 2016). Here we use the term compatibility, as advised in the GAW Report No. 229 (2016), to describe the difference between two measurements, rather than the absolute accuracy of those measurements. The specific compatibility requirements for urban environments, based on this study, are discussed in Section 4. The calibration protocol for the INFLUX sites is described in Richardson et al. (2016). Prior to deployment and following any manufacturer repairs, the instruments are calibrated for slope and offset in the laboratory using 3 to 5 NOAA-calibrated tanks, and at each site, one or two NOAA-calibrated tanks are sampled daily for 10 min as field offset calibration points.

Six sites include co-located flask measurements (Turnbull et al., 2012) taken in the afternoon (1400–1600 LST), with comparisons yielding mean differences of 0.18 ± 0.55 ppm CO_2, 0.6 ± 5.0 ppb CH_4, and –6 ± 4 ppb CO for the period May 2011 – June 2016 (Richardson et al., 2016). Additionally, round robin tests with three NOAA-calibrated tanks were performed at all INFLUX tower sites, yielding network averaged errors of –0.09 ± 0.11 ppm CO_2, 0.2 ± 0.4 ppb CH_4 and 0 ± 2 ppb CO in the November 2013 tests (Richardson et al., 2016). Taking the magnitude of the largest of these results as the uncertainty bound, the compatibility of the values reported in this paper are 0.18 ppm CO_2, 0.6 ppb for CH_4, and 6 ppb for CO.

2.3 Numerical modeling system: Hestia and WRF-FDDA-LPDM

Hestia (Zhou and Gurney, 2010; Gurney et al., 2012), a building-level resolution inventory product for the Indianapolis area, is used as an estimate of anthropogenic CO_2 emissions. Hestia combines several datasets such as energy consumption, traffic data, industrial productivity, and electricity generation from the power plant, with models such as a building energy model. The Hestia product covers Marion county and the other eight surrounding counties and includes diurnal and seasonal variability to compute hourly emissions for any day of the year for a variety of economic sectors at the building/street scale. The CO_2 emissions are available for eight different sectors of economic activity: airport, commercial, industrial, mobility (on-road vehicles), nonroad (vehicles), residential, utility, and railroad. The 2014 release of Hestia describing emissions from 2013 is used in this paper.

The Weather Research Forecasting model (WRF version 3.5.1) modeling system uses a Four-Dimensional Data Assimilation (FDDA) technique, originally developed and tested for the Fifth-Generation Penn State/NCAR Mesoscale Model (Stauffer and Seaman 1994, Deng et al. 2004) and implemented into WRF (Deng et al. 2009) assimilating the meteorological measurements from WMO surface stations as well as vertical profiles from radiosondes. The WRF-FDDA system has been used to produce optimal dynamic analyses for air quality applications (Rogers et al. 2013), and used over the city of Davos, Switzerland, in a project to quantify urban emissions of CO_2 (Lauvaux et al., 2013). It has also been used for an aircraft-based estimate of total methane emissions from the Barnett Shale region (Karion et al. 2015). The simulation domain for the current study encompasses Indianapolis and the surrounding area in a nested mode at 9km, 3km, and 1km resolutions, with the domains covering 900 × 900 km, 297 × 297 km, and 87 × 87 km, respectively. The atmospheric boundary layer scheme used is the Mellor-Yamada-Nakanishi-Niino (MYNN) 2.5 scheme (Nakanishi and Niino, 2004) coupled to the simple urban scheme within the Noah land surface model (Chen and Dudhia, 2001). The atmospheric vertical column was described by 60 levels, with 40 levels in the lower 2 km, the first level being at about 6 m above ground. We use 3-hourly North America Regional Reanalysis (NARR) analyses at 40 × 40-km resolution for the initial conditions and lateral boundary conditions for all WRF simulation. The NARR analyses were downloaded from the Research Data Archive maintained by the Computational and Information Systems Laboratory at the National Center for Atmospheric Research. The influence functions, representing the relationship between mole fractions at the tower locations and their related flux footprints at the surface, were simulated at 1-km resolution over the inner model domain with the Lagrangian Particle Dispersion Model (LDPM) (Uliasz, 1994; Lauvaux et al., 2012). 6300 particles are released incrementally at equal intervals over one-hour periods at the inlet heights at each of the towers. Inputs to the LPDM include mean winds (u,v,w), potential temperature, and turbulent kinetic energy from WRF-FDDA-CO_2 system. Multiplying the influence functions for afternoon hours (1700 – 2100 UTC) during the period 1 January – 30 April 2013 by the total emissions from Hestia (using the afternoon average for each day), we obtain expected mean CO_2 dry mole fraction at the towers for the period.

2.4 Wind measurements

The wind data used in this study are measured at the Indianapolis International Airport (KIND), outside the southwest corner of the city. The data are part of the Integrated Surface Dataset (ISD) (https://www.ncdc.noaa.gov/isd). The weather station at the airport uses the Automated Surface Observing System (ASOS). The complete description of ASOS type stations is available at http://www.nws.noaa.gov/asos/pdfs/aum-toc.pdf. The accuracy of wind speed is ±1.0 ms^{-1} or 5% (whichever is greater) and the accuracy of wind direction is 5 degrees when wind speed is ≥ 2.6 ms^{-1}. Wind directions are not reported for periods in which the wind speed is less than 1.6 ms^{-1}. The height of the wind instrument is about 10 m AGL. The wind data reported in ISD are the wind data at a single point in time recorded within the last 10 minutes of an hour.

2.5 Analyses

Prior to determining the enhancement in urban CO_2, CO and CH_4 dry mole fractions, we first identify well-mixed, steady-state atmospheric conditions. Well-mixed conditions are more tractable for interpretation and for comparison to mesoscale atmospheric model simulations. Furthermore, the rapid morning growth of the convective ABL causes rapid changes in mole fraction caused by entrainment, potentially masking spatial differences caused by surface fluxes. Well-mixed daytime conditions also alleviate sensitivity to nearby point sources. Here we use the term "steady state" to describe conditions under which the boundary layer depth and greenhouse gas mole fractions are not changing quickly. Composited diurnal cycles of CO_2 in July at the WLEF tower in Wisconsin indicate that the atmosphere is generally well-mixed between 1700 and 2100 UTC (1200–1600 LST) (Bakwin et al., 1998, Figure 1d). For the majority of the analyses in this paper, we consider the afternoon average to be the average over the period 17:00:00–20:59:59 UTC, which for brevity, we refer to as 1700–2100 UTC (1200–1600 LST). In Section 3.2.1, we quantify the effect of variable CO_2 mole fraction in the afternoon by considering different time periods, including a time-lagged version.

We choose one site to serve as a background, upwind boundary condition. The dry mole fractions observed at this site are subtracted from all other sites' mole fractions to isolate the enhancement in mole fraction caused by emissions within the city. The results leading to this choice are described in Section 3.1.

We use temporal averaging to quantify the mole fraction enhancements that result from urban emissions. Afternoon averages and a 15-day running average are both examined over the entire three-year record of measurement. A four-month average (January through April 2013) during the dormant season is used to quantify the long-term mole fraction enhancements. This period is chosen to take advantage of the large number of observation sites available and to avoid complications caused by biogenic fluxes that exist during summer months. In the dormant season Turnbull et al. (2015) show that the total CO_2 is an appropriate proxy for fossil-fuel CO_2, at least for Indianapolis and with a local background site. The four-month average mole fractions are also examined as a function of wind direction to quantify variability in the enhancement caused by changing winds. We also compare the four-month average observed CO_2 mole fraction enhancements at each tower site to the mole fraction enhancements simulated by the numerical modeling system.

Finally, we examine the sensitivity of our CO_2 results to variability in maximum sampling altitude and time of day used for comparisons. Long-term differences in CO_2 mole fraction as a function of height are studied at

three towers where multi-level measurements were collected. We use those long-term vertical differences to estimate the mole fractions we would expect across the network if all CO_2 measurements were collected at the same altitude above ground. Similarly, a number of different definitions of well-mixed, steady-state ABL mole fractions are used to determine sensitivity of our results to that choice.

3 Results

3.1 Background sites

Next we evaluate the suitability of Site 01 and Site 09 as background sites by considering the difference between the CO_2 mole fraction measured at each site for each afternoon hour and the minimum mole fraction across the INFLUX tower network measured at the same hour for the period 1 January – 30 April 2013. In **Figure 4a**, the cumulative fraction of afternoon hours of observed CO_2 mole fraction enhancement above a given level is shown. The ideal background site would measure the lowest CO_2 mole fraction at all times (in the dormant season), within the measurement noise. Of course, the perfect background site does not exist, as this would require the wind to always originate from the predominant wind direction and that there were no local sources near the background site. For 43% of the afternoon hours Site 01 measures within 0.2 ppm of the lowest CO_2 amongst the INFLUX towers. Site 09 is less often most appropriate as a background site, but not drastically so. For 39% of the afternoon hours, Site 09 measures within 0.2 ppm of the lowest. In comparison, the other INFLUX sites measure within 0.2 ppm of the lowest site between 0 and 19% of the afternoon hours.

When categorized into subsets during which the wind is from the southeast, southwest and northwest quadrants (**Figure 4b**), Site 09 is further from the lowest value when the wind is from the urban area (i.e., from the southwest) and Site 01 shows evidence of a source(s) to the southeast, most likely attributable to the Eagle Valley Power Plant, 10 km to the south. During this period, the wind comes from the northeast less than 8% of the time; thus the CO_2 enhancement from that direction is not considered. In general, the best background choices are Site 01 in general, Site 01 (when the wind is from the SW or NW), and Site 09 (when the wind is from the SE or NW). For each of these cases, the site in question is within 0.2 ppm of the lowest INFLUX site 42–47% of the afternoon hours. We consider Site 01 as the background site for the purpose of comparison in this paper. As will be shown in Section 3.2, the mean dormant-season afternoon difference between the CO_2 measured at Site 01 and Site 09 is small, 0.3 ppm. Thus, in terms of the time-averaged spatial results presented in this paper, choosing Site 01 as the only background site is not likely to significantly affect the results. However, if considering the temporal variability of mole fraction enhancements, the choice of background may play a more important role.

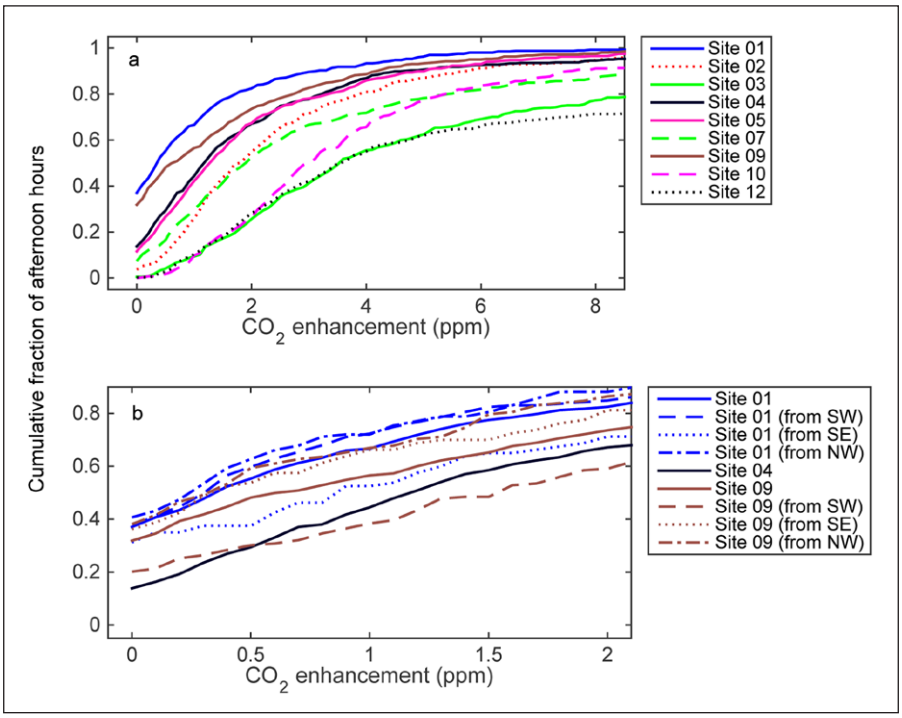

Figure 4: Cumulative fraction of afternoon hours of observed CO_2 mole fraction enhancement above a given level. a) CO_2 enhancement for all sites. Here enhancement is the difference between each site and the INFLUX network minimum for that hour. The averaging period is 1 January – 30 April 2013. Site details are listed in Table 1. Sites 01 and 09 are considered potential background sites. **b)** As in a), but for Site 01 and 09 when the wind is from the southeast (90–180°), from the southwest (180–270°), and from the northwest (270–360°). During this period, the wind comes from the northeast less than 8% of the time; thus the CO_2 enhancement from that direction is not considered. The results for Site 04 averaged over all wind directions are shown for comparison. DOI: https://doi.org/10.1525/elementa.127.f4

3.2 Urban greenhouse gas mole fractions: temporal and spatial cycles

3.2.1 Daytime dormant-season CO_2 dry mole fraction

As an example of the daily afternoon-averaged (1700–2100 UTC, 1200–1600 LST) CO_2, shown in **Figure 5a** are four weeks of data (1 – 28 January 2013). It is apparent that Site 01 generally measures the lowest during the period, except for 24 January for which Site 09 measures the lowest. The highest peak is measured at Site 03 on 8 January, but throughout the period there are days for which five different sites (Sites 02, 04, 07, 10, and 12) measure the highest CO_2. There is a period of four days (19 – 22 January) during which the CO_2 is consistently low at all of the sites. The wind speed measured at the Indianapolis International Airport (**Figure 5d**) is persistently high during this period compared to the rest of the four weeks, consistent with increased mixing of the boundary layer air, and thus lower mole fractions.

Shown in **Figure 6a** is the time series of daily afternoon-averaged CO_2 at INFLUX sites for a period of three years (1 January 2011 – 31 December 2013). Variability at various time scales is apparent. To illustrate the large variability in mole fractions, the two-sigma range (95%) of the daily CO_2 values throughout the measurement period is within 374–418 ppm (44 ppm range) for Site 02. The urban enhancement of CO_2, defined here as the difference between the afternoon-averaged CO_2 measured at a particular site and that measured at the background site (Site 01), is relatively small compared to the range of CO_2 values measured and it is difficult to distinguish between urban and background sites in **Figure 6a**. In general, the urban enhancement observed varies depending on the emissions and the weather conditions (e.g., wind speed and boundary layer depth). 90% of the dormant season (1 January – 30 April 2013) afternoon-averaged CO_2 enhancements above the background site (Site 01) for Site 02 are between –2.41 and 7.00 ppm. For Site 03, 90% of the enhancements are between –0.34 and 9.64 ppm CO_2. In terms of detectability requirements, we instead consider the magnitude of the differences. On 90% of afternoons, the magnitude of the differences between Site 02 and Site 01 is greater than 0.47 ppm, while the compatibility of the measurement is 0.18 ppm CO_2.

In order to visualize the difference between the urban sites from the background sites as a function of time, further averaging is necessary. The daily CO_2 mole fractions, smoothed with a 15-day running mean filter, are shown in **Figure 7a**. In general, with this degree of averaging, the CO_2 shows coherent fluctuations across all of the sites, dominated presumably by variations in the hemispheric flux variations and synoptic-scale transport, rather than by the urban effects. Temporal variability is apparent at multiple scales: synoptic, seasonal, and inter-annual. On the synoptic scale of several days, weather patterns change, leading to differences in boundary layer depth, wind speed and direction and solar radiation, etc., and consequently, the CO_2 is observed to change coherently across all sites. Typical seasonal patterns of hemispheric growing-season CO_2 drawdown and dormant-season respiration are apparent as well. The seasonal minimum and maximum, determined by evaluating a 61-day running mean, occurs about August 1 and December 15, respectively. The growing-season CO_2 drawdown varies considerably amongst the observed years; the seasonal amplitude (defined as the difference between the dormant-season maximum and the previous growing season minimum) is 26/20/33 ppm CO_2

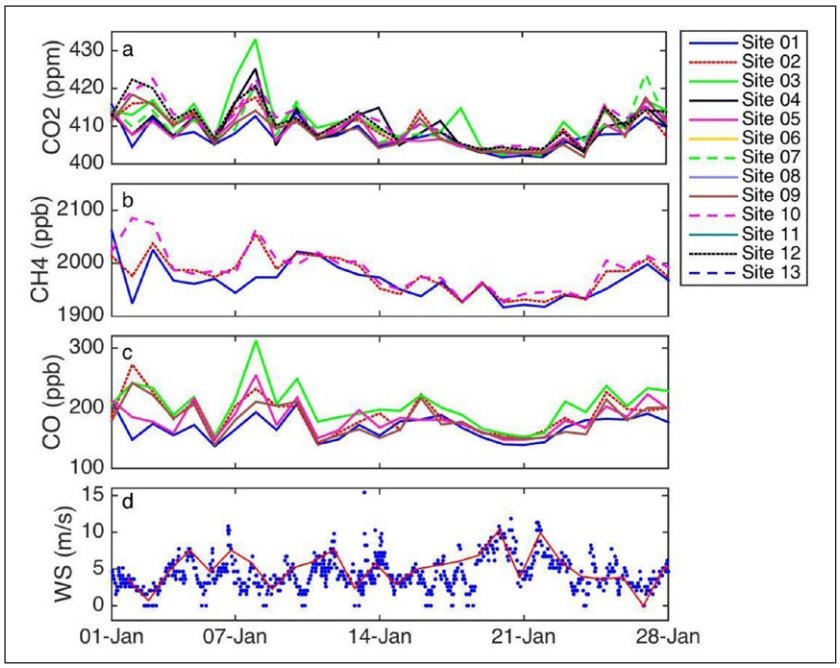

Figure 5: Afternoon-averaged daily mole fractions and wind speed for 1 – 28 January 2013. a) CO_2, **b)** CH_4 and **c)** CO. The data from the tallest measurement height at each tower is used; the measurement heights range from 39 to 136 m AGL (Table 1). Other site details are listed in Table 1 as well. **d)** Wind speeds (WS) measured at the Indianapolis airport for all hours (blue dots) and afternoon-averaged (red line). DOI: https://doi.org/10.1525/elementa.127.f5

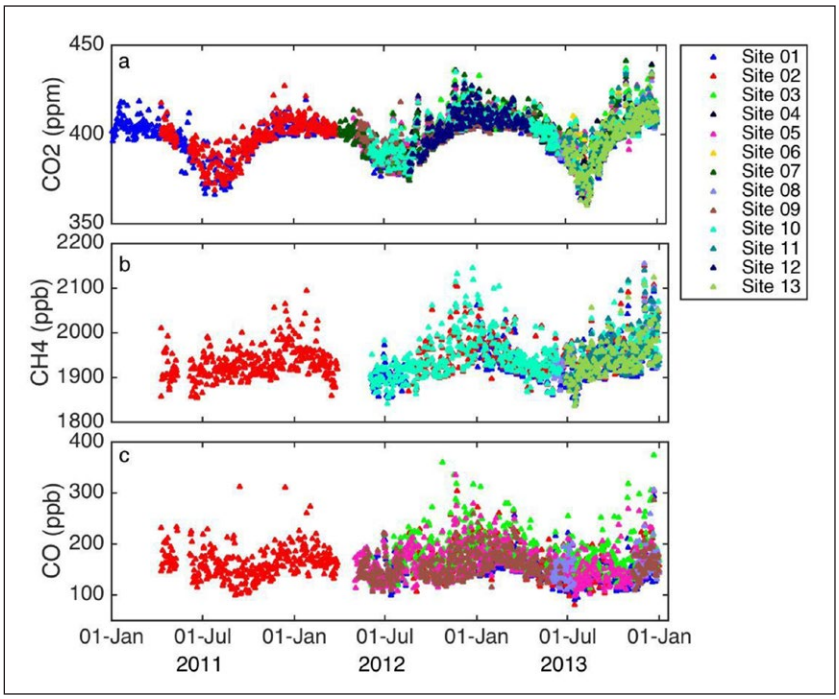

Figure 6: Afternoon-averaged daily mole fractions for the INFLUX tower sites for January 2011 – December 2013. a) CO_2, **b)** CH_4, and **c)** CO. The data from the tallest measurement height at each tower is used; the measurement heights range from 39 to 136 m AGL (Table 1). Other site details are listed in Table 1 as well. DOI: https://doi.org/10.1525/elementa.127.f6

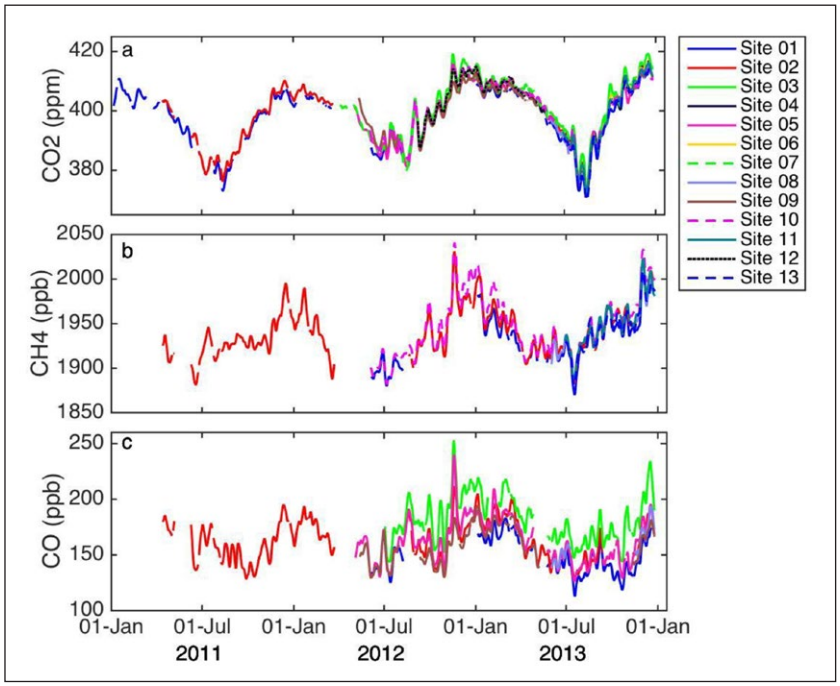

Figure 7: Afternoon-averaged daily mole fractions for January 2011 – December 2013, with 15-day smoothing applied. a) CO_2, **b)** CH_4, and **c)** CO. The data from the tallest measurement height at each tower is used; the measurement heights range from 39 to 136 m AGL (Table 1). Other site details are listed in Table 1 as well. DOI: https://doi.org/10.1525/elementa.127.f7

for the years 2011/2012/2013, respectively, at Site 01. This pattern does not vary appreciably among the sites; at Site 02, the seasonal amplitudes are 26 and 31 ppm for 2011 and 2013, respectively (2012 is not available). The decreased drawdown in 2012 is visible even in the unsmoothed afternoon-averaged CO_2 data (**Figure 6a**) and may be correlated with drought conditions observed that year; while the climatic average monthly precipitation in Indianapolis for May – July is 11.7 cm, only 3.1 cm was measured in 2012 (http://www.crh.noaa.gov).

Averaging over a period of four months (1 January – 30 April 2013) yields a clear spatial pattern induced by the city in the CO_2 signals. Dormant-season time-averaged CO_2 enhancements for each site above the background site (Site 01) are shown in **Figure 8** and listed in **Table 2**. The downtown site (Site 03) measures the largest mean CO_2, 2.9 ppm higher than the background site, whereas Site 02 measures 1.4 ppm larger than the background site. Site 09 measures only 0.3 ppm larger than the background site; this site only occasionally captures the urban plume and there is not a large constant local source of CO_2. The other sites fall between these extremes.

In the above analysis we have used the same averaging interval (1700–2100 UTC) for all the sites. In reality, the CO_2 dry mole fraction changes at the background site while the air mass advects to the downwind sites. In order to quantify this effect, we consider different definitions of well-mixed, steady-state conditions, including a time-lagged version. Shown in **Figure 9** is the observed time-averaged afternoon CO_2 dry mole fraction above background, averaged over different periods of the day (1700–2100 UTC, 2000–2300 UTC, and 2200–2300 UTC). The difference between the result using the averaging interval of 2000–2300 UTC and that using 1700–2100 UTC (the default averaging interval) is +0.2 ppm (ranging from 0.0 to 0.4 ppm) and the difference between using 2200–2300 UTC compared to using the default averaging interval is +0.4 ppm (ranging from 0.2 to 0.9 ppm), where both values are averaged across all sites. These differences in the enhancements above background are attributable to site-to-site differences in the timing of the dilution of the accumulation of emissions in the stable nocturnal boundary layer by the convective growth of the ABL. Rural sites (e.g., Site 01) exhibit a delay in the growth of the ABL relative to the urban sites.

The distance between Site 01 and the other sites is 27–66 km (**Figure 2**). Median near-surface afternoon wind speeds at the Indianapolis Airport are 5.3 ± 2.6 ms^{-1}. Thus a reasonable amount of time for air masses to traverse the distance between Site 01 and Site 02 (42 km) is 1.5–4.3 hr, for example. The actual range of transit times is much larger; in calm winds, an air mass starting at Site 01 in the beginning of the afternoon does not even reach the downwind sites during the same afternoon. But to approximate the effect on the CO_2 dry mole fraction above background, we consider a time-lagged case, subtracting the CO_2 at 1900–2000 UTC at Site 01 from the other sites' CO_2 three hours later at 2200–2300 UTC. The difference

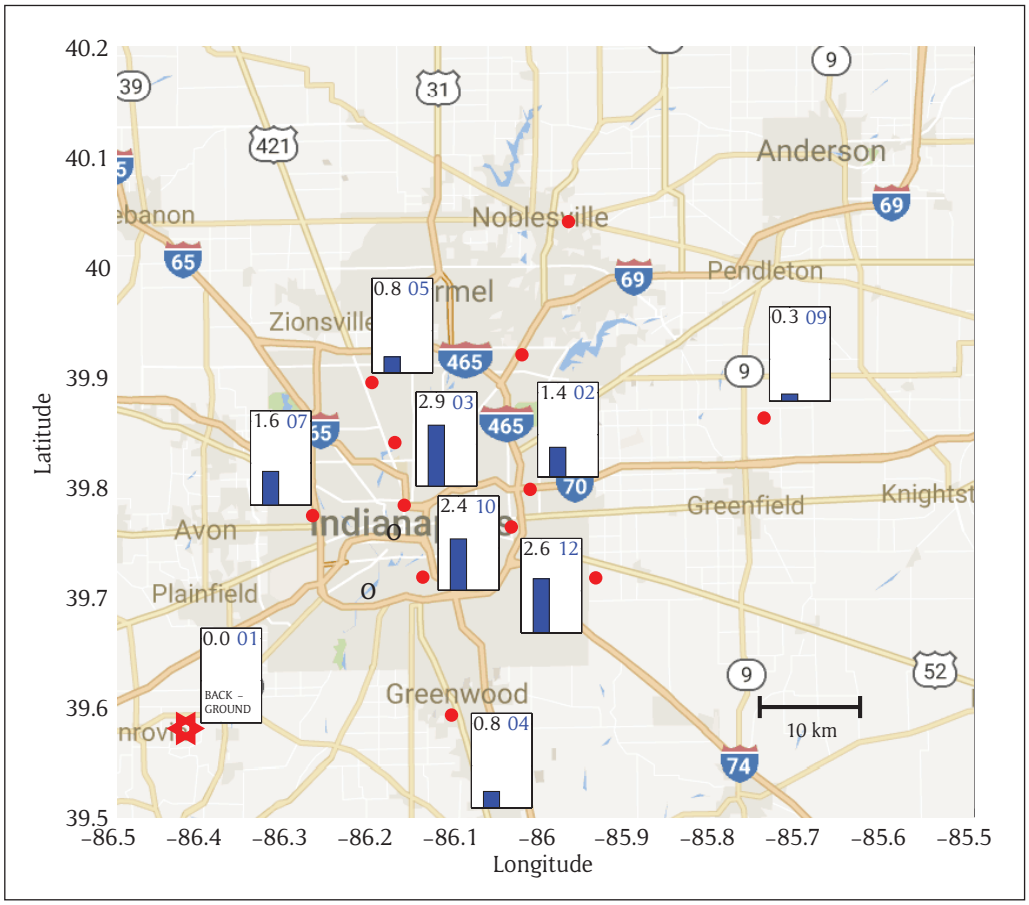

Figure 8: Observed time-averaged afternoon CO_2 dry mole fraction above background (Site 01). The averaging period is 1 January – 30 April 2013. The site number is shown in the upper right corner of each plot and the average observed CO_2 above background (in ppm) in the upper left corner. The full y-axis scale for the plots is 4.5 ppm CO_2. Red filled circles indicate the locations of the sites, with the background Site 01 indicated by a red star. Time frame is chosen to minimize biogenic signals and maximize the number of sites with available data. Sites with less than 75% data availability during the selected time period are excluded. DOI: https://doi.org/10.1525/elementa.127.f8

Table 2: Observed time-averaged CO_2 mole fraction above background (Site 01) for INFLUX tower sites, in order from least to greatest observed urban enhancement. The averaging period is 1 January – 30 April 2013. DOI: https://doi.org/10.1525/elementa.127.t2

	Site 01	Site 09	Site 04	Site 05	Site 02	Site 07	Site 12	Site 10	Site 03
Maximum sampling height (m AGL)	121	130	60	125	136	58	40	40	54
Average CO_2 above background at maximum sampling height (ppm)	–	0.3	0.8	0.8	1.4	1.6	2.5	2.5	2.9
Approximated average CO_2 above background at 40 m AGL (ppm)	–	0.3[1]	0.5 – 0.7[1,2]	0.8 – 1.5[1,2]	2.2	1.3 – 1.4[1,2]	2.1	2.1	3.5

[1]Gradient measured at Site 01 is used to approximate the gradient at this site.
[1,2]The range of values shown originates from using the gradients measured at Site 01 and Site 02 (Figure 14).
Note that the background value at Site 01 is 0.4 ppm higher at 40 m AGL compared to 121 m AGL.

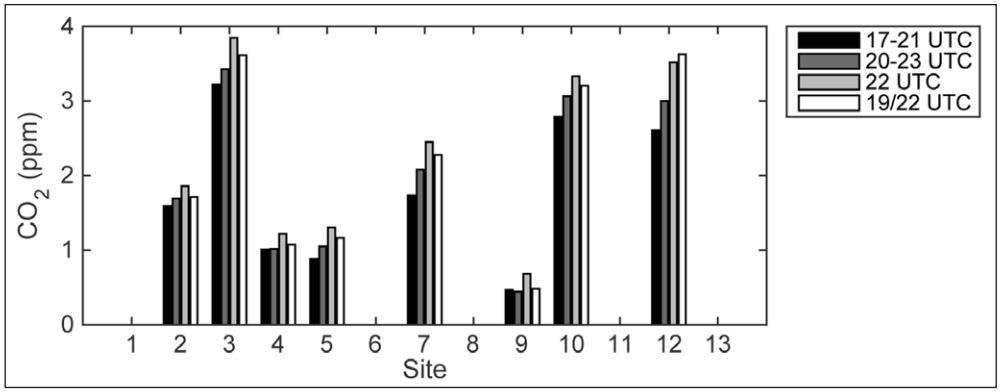

Figure 9: Observed time-averaged afternoon CO_2 dry mole fraction above background (Site 01). The averaging period is 1 January – 30 April 2013. Bars indicate different daily averaging intervals (black: 1700–2100 UTC (1200–1600 LST), dark gray: 2000–2300 UTC (1500–1800 LST), light gray: 2200–2300 UTC (1700–1800 LST)), and a time-lagged version in which the CO_2 dry mole fraction at Site 01 at 1900–2000 UTC (1400–1500 LST) is subtracted from the other sites' CO_2 dry mole fraction at 2200–2300 UTC (1700–1800 LST) (white bar). Sites 06, 08, 11, and 13 were not yet deployed during this period. DOI: https://doi.org/10.1525/elementa.127.f9

between this result and that using 1700–2100 UTC as the averaging interval, averaged across all sites, is +0.4 ppm (ranging from 0.0 to 1.0 ppm at the different sites). Overall, the time averaging choice has a significant impact (0.4 ppm is 25% of the enhancement averaged over all of the sites of 1.6 ppm), but the spatial pattern of the urban enhancement is similar in the tested cases.

3.2.2 Daytime dormant-season CH_4 dry mole fraction

The daytime afternoon-averaged CH_4 mole fraction is shown in **Figure 5b** for 1 – 28 January 2013. As for CO_2, Site 01 most often measures the lowest CH_4 (for the three sites with available data during this period). Site 10, near the large city landfill, measures the highest CH_4 and the period 19 – 22 January measures low CH_4 at all of the sites.

When we examine the entire three-year period, the variability is large and the urban effect is difficult to discern (**Figure 6b**); the two-sigma range of the CH_4 measurements at Site 02 is within 1873–2046 ppb CH_4 (range = 173 ppb). Smoothing with a 15-day filter, there is temporal variability at various scales and the coherence between the sites is clear (**Figure 7b**), as for CO_2. Seasonal amplitudes are 80 and 86 ppb for the years 2012 and 2013, respectively, at Site 01 (2011 is not available), and 42 and 86 ppb for the years 2011 and 2013 at Site 02 (2012 is not available). The synoptic-scale amplitudes are a larger fraction of the seasonal signal, compared to CO_2. The seasonal cycle is also shifted compared to the seasonal cycle of CO_2, with the maximum occurring around November 15 and the minimum around August 15. That minimum corresponds to the time of year for maximum OH, the dominant CH_4 sink, as seen for a range of hydrocarbons in the northern hemisphere (Swanson et al., 2003).

The urban signal is detectable in the CH_4 signal, after averaging each site for the period 1 January – 30 April 2013 (**Figure 10**). The time-averaged CH_4 mole fraction above the background site varies from 5 ppb for Site 13 (southeast of the city, in an agricultural area) to 21 ppb for Site 10 (typically downwind of the South Side Landfill).

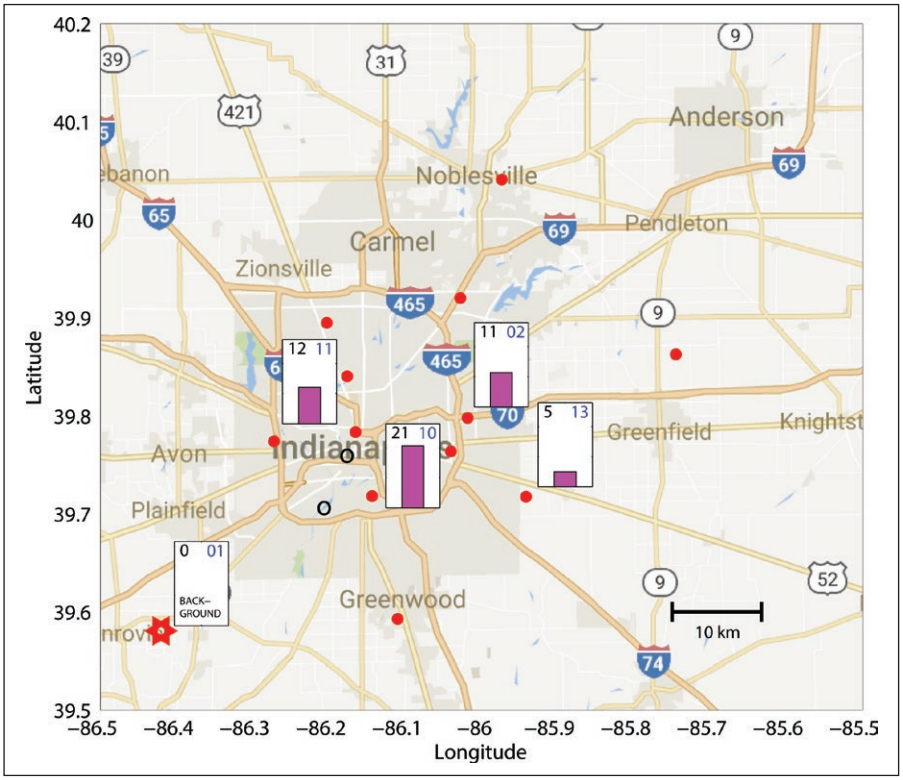

Figure 10: Observed time-averaged afternoon CH_4 dry mole fraction above background (Site 01). The averaging period is 1 October – 31 December 2013. The site number is shown in the upper right corner of each plot (in blue) and the average observed CH_4 above background (in ppb) in the upper left corner. The full y-axis scale for the plots is 28 ppb CH_4. Red filled circles indicate the locations of the sites, with the background Site 01 indicated by a red star. Time frame was chosen to maximize the number of sites with available data. Sites with less than 75% data availability during the selected time period were excluded. DOI: https://doi.org/10.1525/elementa.127.f10

In terms of the range of signals, 90% of the dormant season (1 January – 30 April 2013) afternoon-averaged CH_4 enhancements above the background site (Site 01) for Site 02 are between −13.3 and 35.5 ppb. On 90% of afternoons, the magnitude of the differences between Site 02 and Site 01 is greater than 2.2 ppb CH_4.

3.2.3 Daytime dormant-season CO dry mole fraction

Examining the CO mole fraction measured at the INFLUX sites for 1 – 28 January 2013 (**Figure 5c**), there are similarities with the CO_2 and CH_4 results. Site 01 again measures the lowest mole fractions. There is a large peak particularly at the downtown Site 03 on January 8 (Site 03 measures 119 ppb higher CO than Site 01 on this afternoon) and a period of overall decreased mole fractions on 19 – 22 January (the range amongst the INFLUX sites is only 15 ppb). Over the three-year period, the CO variability from day to day is large compared to the seasonal cycle (**Figure 6c**), consistent with the much shorter photochemical lifetime for CO, compared with the other two gases (Mao and Talbot, 2004). As discussed by Jobson et al. (1999) there is a well-defined (inverse) relationship between lifetime of trace gases and their atmospheric variability. The range of CO values measured at Site 02 is 114–227 ppb for 2-sigma (95%) of the values. The smoothed daily afternoon-averaged CO mole fractions are shown in **Figure 7c**. The seasonal maximum occurs around December 15, but the minimum is too variable to determine a specific date range applicable for all three years.

The time-averaged (1 January – 30 April 2013) CO above the background site varies from 5 ppb for Site 09 to 29 ppb for the downtown Site 03 (**Figure 11**). 90% of the dormant-season afternoon-averaged CO enhancements above the background site (Site 01) for Site 02 are between −13 and 53 ppb. For Site 03, the enhancements are larger, with 90% being between 6 and 79 ppb CO. In terms of detectability requirements, 90% of afternoons exhibit the magnitudes of the differences between Site 02 and Site 01 is greater than 2 ppb. Comparatively, for Site 03 90% of the magnitudes of differences are greater than 11 ppb.

3.2.4 Urban mole fractions as a function of wind direction

Mole fraction differences across the city change, as expected, when segregating them as a function of wind direction. When only considering wind directions from the southwest, Site 02 is downwind of the city, and the average CO_2 mole fraction enhancement is up to 3.3 ppm (**Figure 12a**). When the wind is aligned such that Site 09 captures the urban plume (i.e., from the southwest), Site 09 measures up to 1.6 ppm CO_2 larger than background (**Figure 12b**). An exception is that the CO_2 difference between Sites 09 and 01 is almost 2 ppm when the wind is between 165° and 180° (**Figure 12b**), but with Site 01 higher; this difference is likely attributable to the (coal-fired) Eagle Valley Power Plant that is 10 km south of Site 01.

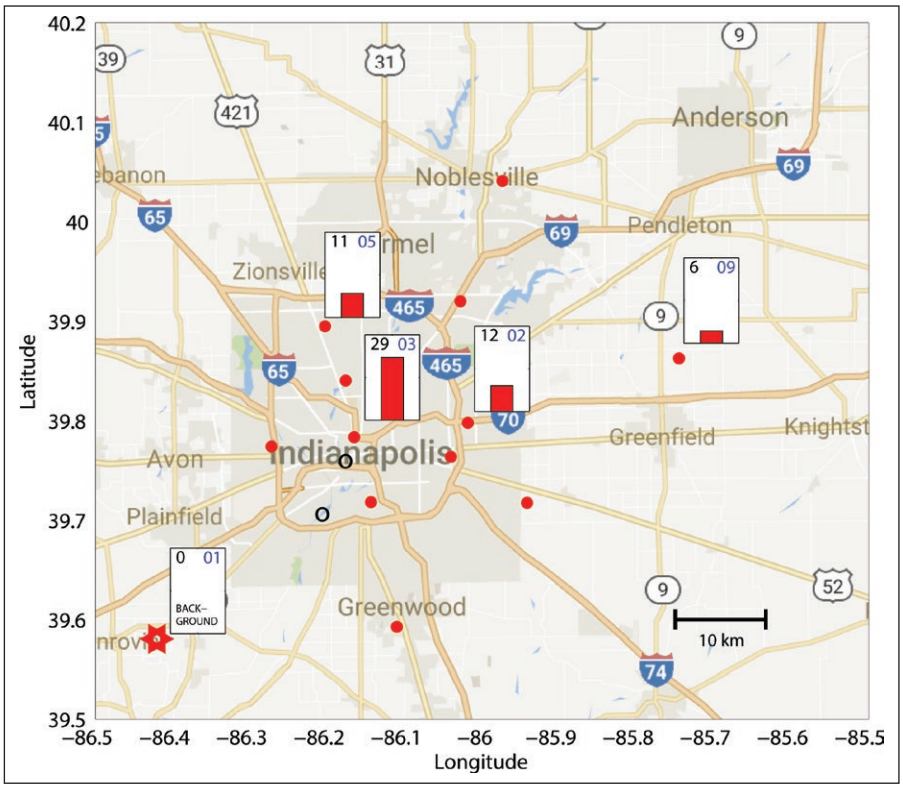

Figure 11: Observed time-averaged afternoon CO dry mole fraction above background (Site 01). The averaging period is 1 January – 30 April 2013. The site number is shown in the upper right corner of each plot (in blue) and the average observed CO above background (in ppb) in the upper left corner. The full y-axis scale for the plots is 40 ppb CO. Red filled circles indicate the locations of the sites, with the background Site 01 indicated by a red star. Time frame was chosen to maximize the number of sites with available data. Sites with less than 75% data availability during the selected time period were excluded. DOI: https://doi.org/10.1525/elementa.127.f11

The CO urban enhancement is up to 34 ppb at Site 02 and 20 ppb at Site 09 when the wind is aligned such that the sites are downwind of the city (**Figure 12c** and **d**). The directions of the enhancements for CO are similar to those for CO_2 except most notably for the lack of a reversed enhancement (Site 01 > Site 09) when the wind is from the south-southeast. In Indianapolis, the CO/CO_2 ratio of vehicular emissions range between 2.2 and 16.2 ppb/ppm with a large single polluter measuring 47.1 ppb/ppm (Vimont et al., 2016). The CO/CO_2 ratio emitted by power plants, however, tends to be either near zero or in the 5 – 7 ppb/ppm range, depending on plant operating conditions (Peischl et al., 2010, Table 3). Our measurements are consistent with the Eagle Valley Power Plant emitting low levels of CO but significant CO_2.

The CH_4 signal for Site 02 originates from a slightly shifted direction compared to CO_2 and CO, with the largest signals from the south-southwest, consistent with a large portion of the CH_4 emissions being from the landfill on the south side of the city (Cambaliza et al., 2015). The magnitude of the enhancement for wind directions between 150 and 300° is up to 21 ppb.

3.3 Time-averaged CO_2 mole fractions: Comparison to modeling results

Combining calculated tower footprints with Hestia emissions, we determine modeled CO_2 as described in Section 2.3 in order to compare with the observed CO_2. The atmospheric inversion approach optimizes the spatially- and temporally-varying emissions by adjusting the emissions in order to minimize the difference between the observed and modeled CO_2 mole fraction. A first step in the process involves comparing the modeled ("forward") CO_2 with the observed. These results, averaged for afternoon hours (1700–2100 UTC) during a dormant period (January – April 2013), are shown in **Figure 13**. In both the modeled and observed results Sites 03 and 10 exhibit the largest enhancements in CO_2, and Sites 09, 04, and 05 show the smallest enhancements. The modeled CO_2 is highly correlated with the observed CO_2, with an r^2 of 0.94 (**Figure 13** inset). This correlation indicates the calculated footprints of the towers are qualitatively correctly sized; e.g., if the Site 09 footprint was actually an order of magnitude larger than modeled here, we would expect the urban signal for Site 09 to be more similar to that of Site 02. The overall magnitude of modeled enhancements is on average, however, only 53% of the observed enhancements (**Figure 13** inset). This result suggests that the either the meteorological model significantly overestimates vertical mixing, the actual emissions in Indianapolis are larger than reported in Hestia, or a combination of both. The mean errors in boundary layer depth, comparing INFLUX WRF modeling results to the Doppler lidar, are small: about 25 m (Deng et al., 2016), so the vertical mixing seems to be accurately modeled, on average. Shown in the **Figure 13** inset is the mean CO_2 mole fraction enhancement using the inverse fluxes (posterior) for 1 Jan-

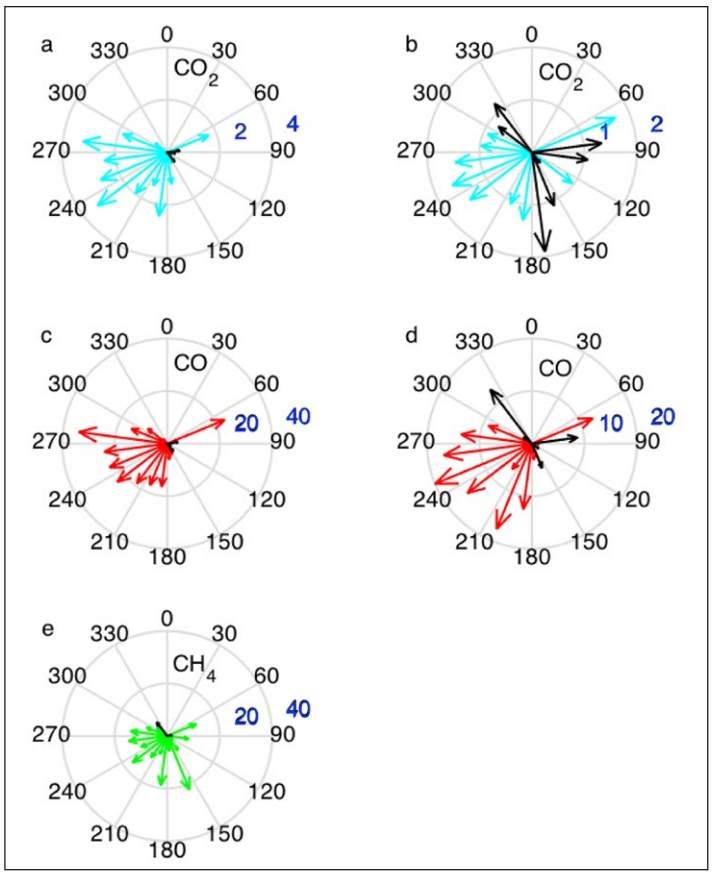

Figure 12: Urban enhancement of greenhouse gases as a function of near-surface wind direction. Here urban enhancement is defined as the mole fraction difference between predominantly downwind site and background Site 01. The averaging period is daytime hours on 1 January – 30 April 2013. Winds are measured at the Indianapolis International airport (http://cdo.ncdc.noaa.gov/qclcd/QCLCD). **a)** CO_2 at Site 02 – CO_2 at Site 01 (ppm), **b)** CO_2 at Site 09 – CO_2 at Site 01 (ppm), **c)** CO at Site 02 – CO at Site 01 (ppb), **d)** CO at Site 09 – CO at Site 01 (ppb), and **e)** CH_4 at Site 02 – CH_4 at Site 01 (ppb). Colored arrows indicate that the downwind site is larger than the background site from that direction, on average. Black arrows indicate that the downwind site is smaller than the background site from that direction, on average. Arrows point to the emission sources. Wind directions occurring on less than 3% of the days are excluded. The urban enhancement magnitude is denoted on the radial scale (in blue); note the differing scales. DOI: https://doi.org/10.1525/elementa.127.f12

uary – 30 April 2013. The posterior modeled enhancements agree well with the observations, as would be expected, and average 95% of the observed enhancements. When averaged over the entire time period of the inversion results in Lauvaux et al. (2016), the inversion results show an increase of about 20% in total emissions from the prior: 5.50 MtC for the period September 2012 – April 2013, compared to 4.56 MtC reported by Hestia. Emissions near the tower sites are increased more than the average pixel across the city, i.e., many pixels have near zero emissions both before and after the inversion. We also note that the inverse emission result also includes nighttime fluxes, which are not significantly modified by the daytime mole fractions at the towers, decreasing the overall change after inversion.

3.4 Vertical profiles of GHG dry mole fraction

3.4.1 CO_2 vertical profiles

Tower heights greater than 100 m AGL are generally considered desirable in order to measure within the well-mixed layer during the day (Bakwin et al., 1998), in order to reduce interpretation problems induced by changing boundary layer depth and to mitigate sensitivity to nearby point sources. Because of the scarcity of tall towers within the city of Indianapolis, however, several towers in the 40–60 m AGL range are utilized in INFLUX. To investigate the ramifications of using shorter towers, composites of the difference between afternoon CO_2 measured at each level and that of the top level are shown in **Figure 14a** for Sites 01, 02, and 03. Averaging over a dormant period (1 November – 31 December 2013), the CO_2 profile at Site 01 is relatively constant compared to the others, with the 40-m level measuring 0.4 ppm higher CO_2 than the top level. The vertical gradient is more pronounced for Site 02, with the 40-m level being 1.2 ppm greater than the top level. Most of the INFLUX towers are between these two towers in terms of urban density. The vertical gradient is largest at Site 03, located downtown with large local emissions. The tower height at that location is 54 m AGL and the difference between the top level CO_2 and

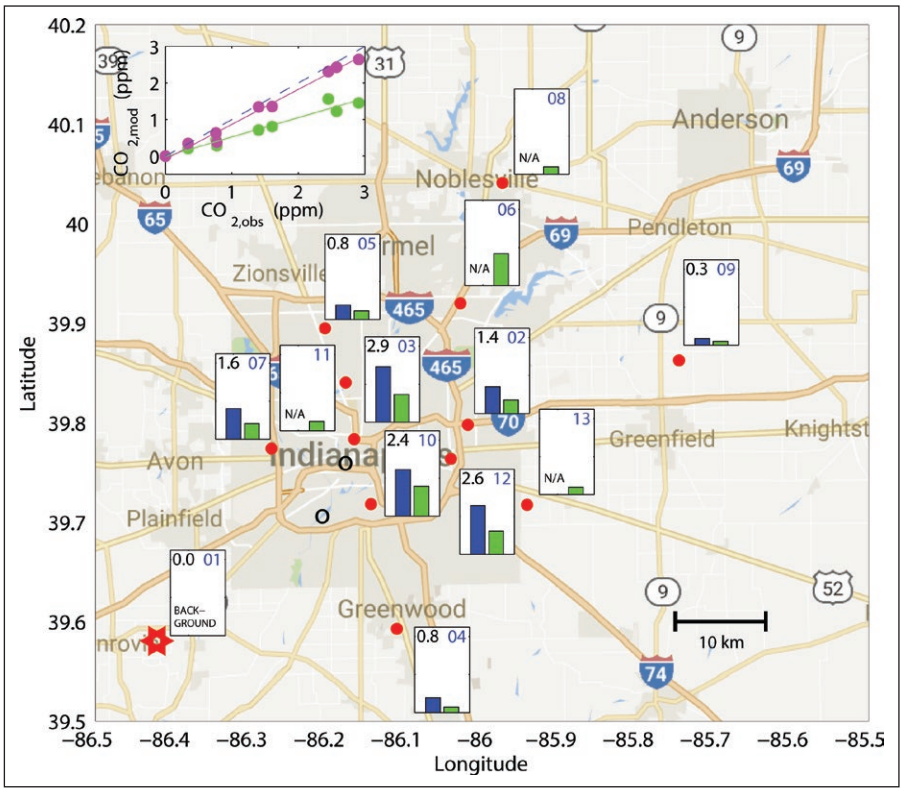

Figure 13: Observed and modeled CO_2 mole fraction above background. Observed (blue) time-averaged afternoon CO_2 mole fraction above background (Site 01) for INFLUX tower sites (1 January – 30 April 2013) at each of the INFLUX towers (represented by red dots), as in Figure 8. Corresponding model results (prior to inversion) using the 2014 release of Hestia describing emissions from 2013 are shown in green. The site number is shown in the upper right corner of each plot (in blue) and the average observed CO_2 above background (in ppm) in the upper left corner. The full y-axis scale for the plots is 4.5 ppm CO_2. Red filled circles indicate the locations of the sites, with the background Site 01 indicated by a red star. Note that not all the sites have CO_2 mole fraction data available during this period; these sites (Sites 06, 08, 11, and 13) are indicated by 'N/A'. The Harding Street Power Plant is indicated by the black circle south of the downtown area; the South Side Landfill is 2 km to the northwest. The smaller C.C. Perry Power Plant is indicated by the black circle near downtown. Shown in the inset is the modeled CO_2 prior to inversion (green) and using optimized fluxes from inversion (magenta) as a function of the observed CO_2. Green and magenta lines show the linear fit and blue dashed line is the 1: 1 line. DOI: https://doi.org/10.1525/elementa.127.f13

that at 40 m is 1.0 ppm. These results are, of course, specific to daytime in the dormant season. Changes in mole fraction as a function of height vary systematically with the sign and magnitude of the local surface fluxes.

The GHG results shown in this study are thus affected by the non-uniformity of tower heights. We now approximate how the results would differ if all the measurements had been at the same height above ground level. We note that the modeling results presented in this paper (Section 3.3) and in Lauvaux et al. (2016) take into account the differing tower heights. One possible approach to address the differing tower heights in the observed results is the virtual tall tower approximation (Davis et al., 2005; Haszpra et al., 2015), in which the CO_2 is normalized to a uniform height for tall towers (>100 m AGL). This approach utilizes a flux-gradient relationship (Wyngaard and Brost, 1984) that is a function of convective velocity scale, boundary layer depth, surface CO_2 flux and surface canopy structure (Wang et al., 2007; Patton et al., 2003). As these measurements are not available at the INFLUX towers, we instead use a simple approach based at CO_2 gradients measured at the sites with multiple tower levels. Seven of the nine INFLUX towers have measurements available at 40–60 m AGL, including three towers with profile measurements. We therefore choose to approximate the CO_2 at 40 m AGL at all the towers for comparison, rather than correcting to >100 m AGL. The gradient between 40 m and the maximum height (>100 m AGL) at Site 01 is 0.5 ppm/100 m and that at Site 02 is 1.3 ppm/100 m. The landcover type at Site 09 is similar to Site 01. We thus use the Site 01 gradient to approximate the difference in CO_2 at 40 m AGL compared to 130 m AGL at Site 09. The urban density at Sites 04, 05 and 07 is between that of Site 01 and Site 02, and a range of values is therefore calculated. The towers at Sites 04 and 07 are 60 m AGL and 58 m AGL, so the adjustments are small (0.2 – 0.3 ppm). The adjustment in the enhancement at Site 05 (with a measurement height of 125 m AGL) to 40 m AGL is in the range of 0.1–0.6 ppm. The CO_2 mole fractions above background at maximum tower height and adjusted (if necessary) to 40 m AGL are both shown in **Table 2**. Note that the background value (Site 01) is 0.4 ppm higher at 40 m AGL compared to 121 m AGL, resulting in a shift in the reported enhancement

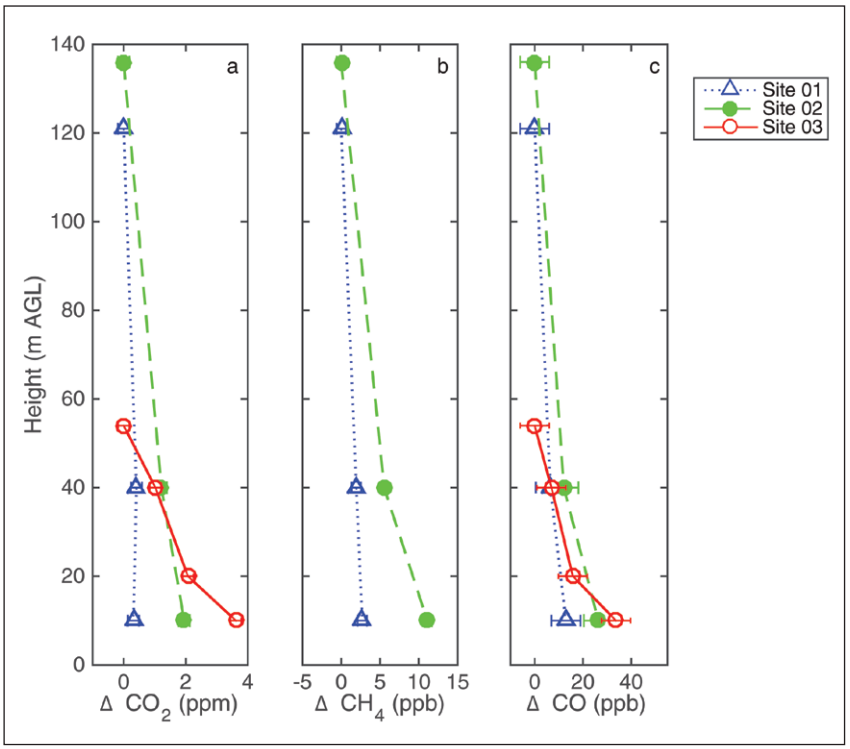

Figure 14: Composites of the vertical changes in greenhouse gas mole fraction. The vertical change is the difference between afternoon **a)** CO_2, **b)** CH_4, and **c)** CO measured at each level and that of the top level. Site 01 is shown as a dotted blue line, Site 02 as a green dashed line, and Site 03 as a solid red line. Shown profiles are using data from two months during the dormant season (1 November – 31 December 2013), as profiles from Sites 01 and 02 were not available for the period 1 January – 2 April 2013. The instrument at Site 03 does not measure CH_4. Here afternoon is defined as 1500–1600 LST. Bars indicate the compatibility of the mole fraction measurements (not visible for CO_2 and CH_4). DOI: https://doi.org/10.1525/elementa.127.f14

even for the sites at which there is a measurement at 40 m AGL (Sites 10 and 12). The spatial mean enhancement is nearly the same: 1.6 ppm compared to 1.7 ppm. While the overall spatial gradients are similar, there are differences for specific towers. For example, the Site 05 enhancement is 0.8 – 1.5 ppm rather than 0.8 ppm, and the Site 02 enhancement is 2.2 ppm rather than 1.4 ppm. At these sites in particular, the enhancement at 40 m AGL is increased by up to 50%, compared to the results using the maximum measurement height at each tower. Thus the height variability has an effect on the results presented here that is similar in magnitude to the effect of time of day for the averaging interval (**Figure 9**).

The 10-m AGL dormant-season mean CO_2 is also shown in **Figure 14a**. Near the source fluxes, the gradients for Sites 02 and 03 are larger: At Site 02 the 10-m CO_2 is 1.9 ppm larger than measured at the top level, and at Site 03 the 10-m CO_2 is 3.6 ppm larger than at the top level. Comparing the 10-m levels at the sites, the Site 02 enhancement at 10 m AGL is 3.2 ppm and that of Site 03 is 7.2 ppm. The measurements at this height are more affected by local signals, i.e., the footprints are smaller (Horst and Weil, 1992) and representative of a smaller area.

3.4.2 CH_4 and CO vertical profiles

The dormant-season averaged profiles of CH_4 mole fraction (**Figure 14b**) indicate a small difference (2.7 ppb) between the CH_4 measured at the lowest level (10 m AGL) compared to the top level (121 m AGL) at the background Site 01. At Site 02, the gradient is larger, with the 10-m AGL CH_4 being 11.1 ppb higher than the highest level. For CO, the dormant-season average at Site 01 is 13 ppb higher at 10 m AGL, compared to the top level (**Figure 14c**). At Site 02 and 03, the differences between the 10 m AGL measurement and that at the top level are 26 and 34 ppb, respectively.

4 Discussion and Conclusions

In this paper, we present three years of CO_2, CH_4, and CO daytime dry mole fractions at towers between 39 and 136 m AGL, observed using cavity ring-down spectrometers at sites in and around Indianapolis, Indiana, in the U.S. Midwest. The differences among the smoothed CO_2 of the sites are small compared to the seasonal- and synoptic-scale variability, showing the importance of the synoptic-scale transport compared to the urban signal. The daily daytime urban signal is overwhelmed by the temporal variability unrelated to urban emissions. Typical synoptic, seasonal, and interannual cycles are apparent at all the sites. The seasonal amplitudes of CO_2 measured in and around Indianapolis average 36 ppm, nearly identical to the average of 35 ppm Miles et al. (2012) observed in the cornbelt region of the U.S. Upper Midwest. However, averaging over several months in the dormant season yields clear urban signals despite the temporal variability. The downtown Site 03 measures 2.9 ppm CO_2 than the background

site, on average. CH_4 and CO are not measured at all of the sites, but for the subset for which these species are measured, the site with the largest magnitude CH_4 difference (21 ppb) from the background site is Site 10. And for CO, the downtown Site 03 measures 29 ppb above the background site. In terms of the range of signals, 90% of the afternoon enhancements at Site 02 are between −2.41 and 7.00 ppm CO_2, between −13.3 and 35.5 ppb CH_4 and between −13 and 53 ppb CO.

The GHG compatibility requirements for global studies (GAW Report No. 213, 2014) are not applicable in urban studies. Instead we define urban compatibility requirements based on this study. To achieve, for example, compatibility at 10% of the mean dormant-season urban signal shown in this study (2.9 ppm CO_2 at Site 03, 21 ppb CH_4 at Site 10 and 29 ppb CO at Site 03), the required compatibility is 0.29 ppm CO_2, 2.1 ppb CH_4 and 2.9 ppb CO. The signals are larger when the data is subset for downwind conditions. Another reasonable metric for the required compatibility is based on the distribution of afternoon-averaged dormant-season enhancements: 90% of the magnitudes of the urban enhancement are greater than 0.47 ppm CO_2, 2.2 ppb CH_4 and 2.3 ppb CO at Site 02. The compatibility for the measurements in this study: 0.18 CO_2, 0.6 ppb CH_4, and 6 ppb CO (Richardson et al., 2016), exceed the requirements for CO_2 and CH_4, but not for CO (based on the mean dormant-season urban signal). We also note that in other cities the compatibility requirements will differ, depending on the magnitude of urban fluxes and specific meteorology (e.g., presence of inversion layer).

The choice of background is crucial for urban GHG emission quantification. Turnbull et al. (2015) show that the total CO_2 is an appropriate proxy for fossil-fuel CO_2 for Indianapolis in the wintertime, but only when using a local background. The total CO_2 is only partially explained by fossil-fuel emissions when using a more distant background. In this paper, defining the urban enhancement as the difference between the mole fraction measured at each site and that measured at an appropriate background site (Site 01) eliminates the effects of synoptic-scale transport and allows interpretation of the urban signal. The location of the background site, however, is a factor in terms of quantification of site-to-site differences. Although Site 01 is the best overall choice of background given the current INFLUX network, it does shows evidence of a source(s) to the southeast, most likely the Eagle Valley Power Plant, 10 km to the south. In terms of the overall spatial patterns presented in this paper, choosing Site 01 as the only background site is not likely to largely affect the results, given that the mean difference between Site 01 and Site 09 is 0.3 ppm. Furthermore, inverse emission results indicate the difference in city emissions between using Site 01 as a background and using either Site 01 or Site 09 depending on the wind direction is low, about 4% (Lauvaux et al., 2016). However, when investigating time-variability in mole fraction enhancements or emissions, the effect may be larger.

Although the vertical gradients in CO_2 can be quite large, the effects of varying tower sampling heights were found to be significant but secondary to the observed spatial gradients for the various tower heights which are between 39 and 136 m AGL. For example, the enhancement of Site 03 compared to Site 01 considering the highest measurement level at both is 2.9 ppm, and for the 40-m measurement, the enhancement is 3.5 ppm. The atmospheric inversion results for INFLUX shown in Lauvaux et al. (2016) use transport resulting from releasing particles from the actual tower sampling heights, but the effect of the various tower heights on modeled emissions is dependent on the ability of the model to properly simulate vertical mixing. If, however, we consider the measurements at 10 m AGL, the Site 03 enhancement is 6.5 ppm, more than double the result for the highest tower measurements, and the results are representative of a smaller area.

Site 02 and Site 09 are both located predominantly downwind of the city. Therefore, the urban enhancements at these two sites can be used to characterize the relationship between the observed atmospheric signals and the distance to the metropolitan area. Subsampling for wind directions such that the sites are downwind of the city increases the urban signal, from 1.4 ppm to 3.3 ppm at Site 02 at the downwind edge of the city, for example. Similarly, the average signal at Site 09 (24 km east of the edge of the city) is 0.3 ppm, but is 1.6 ppm when the wind is aligned such that Site 09 is downwind of the city. Horizontal dispersion of the urban plume and entrainment decrease the signal by 51% over the 24 km between Site 02 and 09 when the wind is from the direction of the city. These results have potential implications for the satellite-based detection of mid- and small-sized cities (without topographical trapping of pollutants). Depending on the distance of satellite tracks from the urban center, this dramatic decrease could be a limiting factor. For example, the OCO-2 orbit tracks are separated by about 170 km (http:/oco.jpl.nasa.gov). Moreover, the results presented here are boundary layer measurements, and column-based measurements would be further diluted.

Similar measurements of urban greenhouse gas mole fractions are being performed in cities around the world. In Paris, Bréon et al. (2015) reported CO_2 mole fraction data for two 30-day periods using five instrumented tower sites. Two of the sites are located in mixed urban-rural areas and two sites used as background are part of the Integrated Carbon Observation System network 20 and 100 km from the urban center. An additional measurement, at the top of the Eiffel Tower, was determined to be poorly represented by the model for most wind speeds and directions. In Los Angeles, CO_2 and CH_4 are being measured at 14 tower and building roof-top sites within and near the Los Angeles basin (https://megacities.jpl.nasa.gov/; Verhulst et al., 2017). McKain et al. (2012) presented CO_2 data from Salt Lake City, Utah, and McKain et al. (2014) described the Boston, Massachusetts, network of five tower- and building-based observations.

The city of Indianapolis is readily detectable by the INFLUX network of in-situ tower-based greenhouse gas mole fraction measurements. The network represents one of the first urban deployments of multiple

high-compatibility sensors. Spatial patterns in the observations are consistent with urban density and confirm the presence of high-resolution information for determination of spatial and temporal variability in emissions via an atmospheric inversion. The observed average dormant season CO_2 dry mole fraction and those predicted by a numerical modeling system are highly correlated. This paper represents an attempt to fully characterize and quantify urban GHG enhancements across space and time in a large metropolitan area.

Data Accessibility Statement

Miles NL, Richardson SJ, Davis KJ, and Haupt BJ, 2017. In-situ tower atmospheric measurements of carbon dioxide, methane and carbon monoxide mole fraction for the Indianapolis Flux (INFLUX) project, Indianapolis, IN, USA. Data set. Available on-line [http://datacommons.psu.edu] from The Pennsylvania State University Data Commons, University Park, Pennsylvania, USA. http://dx.doi.org/10.18113/D37G6P

For further information, see http://sites.psu.edu/INFLUX.

Acknowledgements

D. Sarmiento (The Pennsylvania State University) provided building height analysis. B. Haupt (The Pennsylvania State University) contributed data ingest scripting and data preprocessing. Earth Networks, Inc. provided assistance in site maintenance. The authors would also like to thank J. Miles for help in maintaining the sites.

Funding information

This work is supported by the National Institute of Standards and Technology (Project # 70NANB10H245) and the National Oceanic and Atmospheric Administration (Award # NA13OAR4310076).

Competing interests

The authors have no competing interests to declare.

Contributions

- Contributed to conception and design: KJD, PBS, KG, TL, NLM, SJR, CS, JCT
- Contributed to acquisition of in-situ data: NLM, SJR
- Contributed to acquisition of flask data: JCT, MOC, CS
- Contributed to modeling results: TL, AD, KRG, RP, IR
- Contributed to analysis and interpretation of data: NLM, KJD, TL, SJR, MOC, PBS, CS, JCT, NVB
- Drafted and/or revised article: NLM, KJD, TL

References

Andres, RJ, Fielding, DJ, Marland, G, Boden, TA, Kumar, N and **Kearney, AT** 1999 Carbon dioxide emissions from fossil-fuel use, 1751–1950. *Tellus* **51B**: 759–765. DOI: https://doi.org/10.3402/tellusb.v51i4.16483

Asefi-Najafabady, S, Rayner, PJ, Gurney, KR, McRobert, A, Song, Y, et al. 2014 A multiyear, global gridded fossil fuel CO_2 emission data product: Evaluation and analysis of results. *J Geophys Res Atmos* **119**(17): 10213–10231. DOI: https://doi.org/10.1002/2013JD021296

Bakwin, PS, Tans, PP, Hurst, DF and **Zhao, C** 1998 Measurements of carbon dioxide on very tall towers: Results of the NOAA/CMDL program. *Tellus* **50B**: 401–415. DOI: https://doi.org/10.1034/j.1600-0889.1998.t01-4-00001.x

Bréon, FM, Broquet, G, Puygrenier, V, Chevallier, F, Xueref-Remy, I, et al. 2015 An attempt at estimating Paris area CO_2 emissions from atmospheric concentration measurements. *Atmos Chem Phys* **15**: 1707–1724. DOI: https://doi.org/10.5194/acp-15-1707-2015

Cambaliza, MOL, Shepson, PB, Bogner, J, Caulton, DR and **Stirm, B** 2015 Quantification and source apportionment of the methane emission flux from the city of Indianapolis. *Elem Sci Anth* **3**: 000037. DOI: https://doi.org/10.12952/journal.elementa.000037

Cambaliza, MO, Shepson, PB, Caulton, D, Stirm, B, Samarov, D, et al. 2014 Assessment of uncertainties of an aircraft-based mass-balance approach for quantifying urban greenhouse gas emissions. *Atmos Chem Phys* **14**: 9029–9050. www.atmos-chem-phys.net/14/9029/2014/, DOI: https://doi.org/10.5194/acp-14-9029-2014

Chen, F and **Dudhia, J** 2001 Coupling an advanced land surface–hydrology model with the Penn State–NCAR MM5 modeling system. Part I: Model implementation and sensitivity. *Mon Wea Rev* **129**: 569–585. DOI: https://doi.org/10.1175/1520-0493(2001)129<0569:CAALSH>2.0.CO;2

Ciais, P, Rayner, P, Chevallier, F, Bousquet, P, Logan, M, et al. 2010 Atmospheric inversions for estimating CO_2 fluxes: methods and perspectives. *Climatic Change* **103**: 69–92. DOI: https://doi.org/10.1007/s10584-010-9909-3

Davis, KJ 2005 Well-calibrated CO_2 mixing ratio measurements at flux towers: The virtual tall towers approach. 12th WMO/IAEA Meeting of Experts on Carbon Dioxide Concentration and Related Tracers Measurement Techniques, Toronto, Canada, 15–18 September 2003, WMO GAW Report no. 161, 101–108.

Deng, AJ, Lauvaux, T, Davis, KJ, Gaudet, BJ, Miles, N, et al. 2016 Toward reduced transport errors in a high resolution urban CO_2 inversion system. *Elem Sci Anth*, in press.

Deng, A, Seaman, NL, Hunter, GK and **Stauffer, DR** 2004 Evaluation of inter-regional transport using the MM5/SCIPUFF system. *J Appl Meteor*, **43**: 1864–1886, 2004. DOI: https://doi.org/10.1175/JAM2178.1

Deng, A, Stauffer, DR, Gaudet, BJ, Dudhia, J and **Hacker, J** 2009 Update on WRF-ARW end-to-end multi-scale FDDA system, 10th Annual WRF Users' Workshop, Boulder, CO, June 23, 14 pp. (Available at: http://www2.mmm.ucar.edu/wrf/users/workshops/WS2009/abstracts/1-09.pdf).

Durant, AJ, Le Quere, C, Hope, C and **Friend, AD** 2011 Economic value of improved quantification in global sources and sinks of carbon dioxide. *Philos Trans A*

369: 1967–1979. DOI: https://doi.org/10.1098/rsta.2011.0002

European Commission, Joint Research Centre (JRC)/Netherlands Environmental Assessment Agency (PBL) 2013 Emission Database for Global Atmospheric Research (EDGAR), release EDGARv4.2 FT2010. (Available at: http://edgar.jrc.ec.europa.eu).

GAW Report No. 229 2016 18th WMO/IAEA Meeting on Carbon Dioxide, Other Greenhouse Gases and Related Tracers Measurement Techniques (GGMT-2015), La Jolla, CA, USA, 13–17 September 2015.

Gurney, KR, Mendoza, D, Zhou, Y, Seib, B and **Fischer, M** 2009 The Vulcan Project: High resolution fossil fuel combustion CO_2 emissions fluxes for the United States. *Environ Sci Technol* **43**. DOI: https://doi.org/10.1021/es900806c

Gurney, KR, Razlivanov, I, Song, Y, Zhou, Y, Benes, B, et al. 2012 Quantification of fossil fuel CO_2 emissions on the building/street scale for a large U.S. city. *Environ Sci Technol* **46**: 12194–12202. DOI: https://doi.org/10.1021/es3011282

Haszpra, L, Barcza, Z, Haszpra, T, Pátkai, ZS and **Davis, KJ** 2015 How well do tall-tower measurements characterize the CO_2 mole fraction distribution in the planetary boundary layer? *Atmos Meas Tech* **8**: 1657–1671. DOI: https://doi.org/10.5194/amt-8-1657-2015

Horst, TW and **Weil, JC** 1992 Footprint estimation for scalar flux measurements in the atmospheric surface layer. *Bound Lay Meteorol* **59**: 279–296. DOI: https://doi.org/10.1007/BF00119817

IEA: World Energy Outlook 2008 Organization for Economic Co-operation and Development/International Energy Agency (OECD/IEA), 578 pp.

IPCC: Climate Change 2014 Synthesis Report. Contribution of Working Groups I, II and III to the Fifth Assessment Report of the Intergovernmental Panel on Climate Change [Core Writing Team, Pachauri, RK and Meyer, LA, (eds.)]. IPCC, Geneva, Switzerland, 151 pp.

Jin, S, Yang, L, Danielson, P, Homer, C, Fry, J, et al. 2013 A comprehensive change detection method for updating the National Land Cover Database to circa 2011. *Remote Sens Environ* **132**: 159–175. DOI: https://doi.org/10.1016/j.rse.2013.01.012

Jobson, BT, McKeen, SA, Parrish, DD, Fehsenfeld, FC, Blake, DR, et al. 1999 Trace gas mixing ratio variability versus lifetime in the troposphere and stratosphere: Observations. *J Geophys Res* **104**: 16, 091–16, 113. DOI: https://doi.org/10.1029/1999JD900126

Karion, A, Sweeney, C, Kort, EA, Shepson, PB, Brewer, A, et al. 2015 Aircraft-based estimate of total methane emissions from the Barnett Shale region. *Environ Sci Technol* **49**: 8124–8131. DOI: https://doi.org/10.1021/acs.est.5b00217

Lauvaux, T, Miles, N, Deng, A, Richardson, S, Cambaliza, MO, et al. 2016 High resolution atmospheric inversion of urban CO_2 emissions during the dormant season of the Indianapolis Flux Experiment (INFLUX). *J Geophys Res Atmos* **121**: 5213–5236. DOI: https://doi.org/10.1002/2015JD024473

Lauvaux, T, Miles, NL, Richardson, SJ, Deng, A, Stauffer, DR, et al. 2013 Urban emissions of CO_2 from Davos, Switzerland: The first real-time monitoring system using an atmospheric inversion technique. *J Appl Meteor Climatol* **52**: 2654–2668. DOI: https://doi.org/10.1175/JAMC-D-13-038.1

Lauvaux, T, Schuh, A, Uliasz, M, Richardson, S, Miles, N, et al. 2012 Constraining the CO_2 budget of the corn belt: Exploring uncertainties from the assumptions in a mesoscale inverse system. *Atmos Chem Phys* **12**: 337–354. DOI: https://doi.org/10.5194/acp-12-337-2012

Mao, H and **Talbot, R** 2004 O_3 and CO in New England: Temporal variations and relationships. *J Geophys Res* **109**(D21): 304. DOI: https://doi.org/10.1029/2004JD004913

Marland, G and **Boden, T** 1993 The magnitude and distribution of fossil-fuel-related carbon releases. In NATO ASI Series, The Global Carbon Cycle, edited by Heimann, M, Spring Berlin Heidelberg, **15**: 117–138. DOI: https://doi.org/10.1007/978-3-642-84608-3_5

Marland, G, Rotty, RM and **Treat, NL** 1985 CO_2 from fossil fuel burning: global distribution of emissions. *Tellus* **37B**: 243–258. DOI: https://doi.org/10.1111/j.1600-0889.1985.tb00073.x

Mays, KL, Shepson, PB, Stirm, BH, Karion, A, Sweeney, C, et al. 2009 Aircraft-based measurements of the carbon footprint of Indianapolis. *Environ Sci Technol* **43**: 7316–7823. DOI: https://doi.org/10.1021/es901326b

McKain, K, Wofsy, SC, Nehrkorn, T, Eluszkiewicz, J, Ehleringer, JR, et al. 2012 Assessment of ground-based atmospheric observations for verification of greenhouse gas emissions from an urban region. *Proc Nat Acad Sci* **109**(22): 8423–8428. DOI: https://doi.org/10.1073/pnas.1116645109

Miles, NL, Richardson, SJ, Davis, KJ, Lauvaux, T, Andrews, AE, et al. 2012 Large amplitude spatial and temporal gradients in atmospheric boundary layer CO_2 mole fractions detected with a tower-based network in the U.S. Upper Midwest. *J Geophys Res B* **117**(G01): 019. DOI: https://doi.org/10.1029/2011JG001781

Nakanishi, M and **Niino, H** 2004 An improved Mellor-Yamada Level-3 model with condensation physics: Its design and verification. *Bound Layer Meteor* **112**: 1–31. DOI: https://doi.org/10.1023/B:BOUN.0000020164.04146.98

Nisbet, E and **Weiss, R** 2010 Top-down versus bottom-up. *Science* **328**(5983). DOI: https://doi.org/10.1126/science.1189936

Oda, T and **Maksyutov, S** 2011 A very high-resolution (1 km × 1 km) global fossil fuel CO_2 emission inventory derived using a point source database and satellite observations of nighttime lights. *Atmos Chem Phys* **11**: 543–556. www.atmos-chem-phys.net/11/543/2011/, DOI: https://doi.org/10.5194/acp-11-543-2011

Pacala, SW, Breidenich, C, Brewer, PG, Fung, IY, Gunson, MR, et al. 2010 Verifying greenhouse

gas emissions: Methods to support international climate agreements. Committee on methods for estimating greenhouse gas emissions, National Research Council.

Patton, EG, Sullivan, PP and **Davis, KJ** 2003 The influence of a forest canopy on top-down and bottom-up diffusion in the planetary boundary layer. *Quart J Roy Meteor* **129**(590): 1415–1434. DOI: https://doi.org/10.1256/qj.01.175

Peischl, J, Ryerson, TB, Holloway, JS, Parrish, DD, Trainer, M, et al. 2010 A top-down analysis of emissions from selected Texas power plants during TexAQS 2000 and 2006. *J Geophys Res* **115**(D16): 303. DOI: https://doi.org/10.1029/2009JD013527

Rayner, PJ, Raupach, MR, Paget, M, Peylin, P and **Koff, E** 2010 A new global gridded data set of CO_2 emissions from fossil fuel combustion: Methodology and evaluation, *J Geophys Res* **115**(D19): 306. DOI: https://doi.org/10.1029/2009JD013439

Richardson, SJ, Miles, NL, Davis, KJ, Lauvaux, T, Martins, D, et al. 2016 CO_2, CO, and CH_4 surface in situ measurement network in support of the Indianapolis FLUX (INFLUX) Experiment. *Elem Sci Anth*, under review.

Rogers, RE, Deng, A, Stauffer, DR, Gaudet, BJ, Jia, Y, et al. 2013 Application of the Weather Research and Forecasting Model for air quality modeling in the San Francisco Bay Area. *J Appl Meteor* **52**: 1953–1973. DOI: https://doi.org/10.1175/JAMC-D-12-0280.1

Schuh, AE, Lauvaux, T, West, TO, Denning, AS, Davis, KJ, et al. 2013 Evaluating atmospheric CO_2 inversions at multiple scales over a highly inventories agricultural landscape. *Global Change Biol* **19**(5): 1424–1439. DOI: https://doi.org/10.1111/gcb.12141

Swanson, AL, Blake, NJ, Atlas, E, Flocke, F, Blake, DR, et al. 2003 Seasonal variations of C_2–C_4 nonmethane hydrocarbons and C_1–C_4 alkyl nitrates at the Summit research station in Greenland. *J Geophys Res* **108**(D2): 4065. DOI: https://doi.org/10.1029/2001JD001445

Turnbull, J, Guenther, D, Karion, A, Sweeney, C, Anderson, E, et al. 2012 An integrated flask sample collection system for greenhouse gas measurements. *Atmos Meas Tech* **5**: 2321–2327. DOI: https://doi.org/10.5194/amt-5-2321-2012

Turnbull, J, Sweeney, C, Karion, A, Newberger, T, Tans, P, et al. 2015 Towards quantification and source sector identification of fossil fuel CO_2 emissions from an urban area: Results from the INFLUX experiment. *J Geophys Res Atmos* **120**. DOI: https://doi.org/10.1002/2014JD022555

Uliasz, M 1994 Lagrangian particle modeling in mesoscale applications. In Environmental Modelling II, ed. Zanetti, P, Computational Mechanics Publications, 71–102.

U.S. Energy Information Administration 2016 Available at: http://www.eia.gov/electricity/data/browser/, last accessed 2 October 2016.

Verhulst, KR, Karion, A, Kim, J, Salameh, PK, Keeling, RF, et al. 2017 Carbon dioxide and methane measurements from the Los Angeles Megacity Carbon Project: 1. Calibration, urban enhancements, and uncertainty estimates. *Atmos Chem Phys Discuss*, under review. DOI: https://doi.org/10.5194/acp-2016-850

Vimont, IJ, Turnbull, JC, Petrenko, VV, Place, PP, Karion, A, et al. 2016 Carbon monoxide isotopic measurements in a US urban center confirm traffic emissions as the dominant wintertime carbon monoxide source. *Elem Sci Anth*, under review.

Wang, W, Davis, KJ, Yi, C, Patton, EG, Butler, MP, et al. 2007 Estimating daytime CO_2 fluxes over a mixed forest from tall tower mixing ratio measurements. *Bound Layer Meteor* **124**: 305–314. DOI: https://doi.org/10.1007/s10546-007-9162-0

Wyngaard, JC and **Brost, RA** 1984 Top-down and bottom-up diffusion of a scalar in the convective boundary layer. *J Atmos Sci* **41**: 102–112. DOI: https://doi.org/10.1175/1520-0469(1984)041<0102:TDABUD>2.0.CO;2

Zhou, Y and **Gurney, K** 2010 A new methodology for quantifying on-site residential and commercial fossil fuel CO_2 emissions at the building spatial scale and hourly time scale. *Carbon Manage* **1**(1): 45–56. DOI: https://doi.org/10.4155/cmt.10.7

How to cite this article: Miles, NL, Richardson, SJ, Lauvaux, T, Davis, KJ, Balashov, NV, Deng, A, Turnbull, JC, Sweeney, C, Gurney, KR, Patarasuk, R, Razlivanov, I, Cambaliza, MOL and Shepson, PB 2017 Quantification of urban atmospheric boundary layer greenhouse gas dry mole fraction enhancements in the dormant season: Results from the Indianapolis Flux Experiment (INFLUX). *Elem Sci Anth,* 5: 27, DOI: https://doi.org/10.1525/elementa.127

Domain Editor-in-Chief: Detlev Helmig, University of Colorado Boulder, US

Guest Editor: Paul Palmer, The University of Edinburgh, UK

Knowledge Domain: Atmospheric Science

Part of an *Elementa* Special Feature: Quantification of urban greenhouse gas emissions: The Indianapolis Flux experiment

Submitted: 14 October 2016 **Accepted:** 29 March 2017 **Published:** 13 June 2017

Copyright: © 2017 The Author(s). This is an open-access article distributed under the terms of the Creative Commons Attribution 4.0 International License (CC-BY 4.0), which permits unrestricted use, distribution, and reproduction in any medium, provided the original author and source are credited. See http://creativecommons.org/licenses/by/4.0/.

ELEMENTA Science of the Anthropocene

Elem Sci Anth is a peer-reviewed open access journal published by University of California Press.

OPEN ACCESS